Published in final edited form as:

*J Physiol*. 2021 January ; 599(2): 571–592. doi:10.1113/JP281011.

# Piezo1 channels mediate trabecular meshwork mechanotransduction and promote aqueous fluid outflow

**Oleg Yarishkin**[1,*], **Tam T. T. Phuong**[1,*], **Jackson M. Baumann**[1,2,*], **Michael L. De Ieso**[3], **Felix Vazquez-Chona**[1], **Christopher N. Rudzitis**[1], **Chad Sundberg**[1], **Monika Lakk**[1], **W. Daniel Stamer**[3], **David Križaj**[1,2,4]

[1]Department of Ophthalmology and Visual Sciences, University of Utah, Salt Lake City, UT 84132, USA

[2]Department of Bioengineering, University of Utah, Salt Lake City, UT 84132, USA

[3]Duke Eye Center, Duke University School of Medicine, Durham, NC 27710, USA

[4]Department of Neurobiology and Anatomy, University of Utah School of Medicine, Salt Lake City, UT 84132, USA.

## Abstract

Chronic elevations in intraocular pressure (IOP) can cause blindness by compromising the function of trabecular meshwork (TM) cells in the anterior eye but how these cells sense and transduce pressure stimuli is poorly understood. Here, we demonstrate functional expression of two mechanically activated channels in human TM cells. Pressure-induced cell stretch evoked a rapid increase in transmembrane current that was inhibited by antagonists of the mechanogated channel Piezo1, Ruthenium Red and GsMTx4, and attenuated in Piezo1-deficient cells. The majority of TM cells exhibited a delayed stretch-activated current that was mediated independently of Piezo1 by TRPV4 (Transient Receptor Potential Cation Channel, Subfamily V, Member 4) channels. Piezo1 functions as the principal TM transducer of physiological levels of shear stress, with both shear and the Piezo1 agonist Yoda1 increasing the number of focal cell-matrix contacts. Analysis of TM-dependent fluid drainage from the anterior eye showed significant inhibition by GsMTx4. Collectively, these results suggest that TM mechanosensitivity utilizes kinetically, regulatory and functionally distinct pressure transducers to inform the cells about force-sensing contexts. Piezo1-dependent control of shear flow sensing, calcium homeostasis, cytoskeletal dynamics and pressure-dependent outflow suggests potential for a novel therapeutic target in treating glaucoma.

### Keywords

Trabecular meshwork; mechanosensation; shear stress; ion channel; Piezo1; TRPV4

***Correspondence to:*** Oleg Yarishkin or David Krizaj, 65 N Mario Capecchi Drive, Bldg. 523, Room S4140 JMEC, Salt Lake City, UT 84132.

*Equal contribution.

## Introduction

Glaucoma, the leading cause of irreversible blindness in the developed world, affects ~80 million people worldwide (Jonas et al., 2017). Intraocular pressure (IOP) represents the principal and sole treatable factor for all forms of glaucoma, indicating that this is largely a disease of IOP dysregulation and pathological mechanotransduction (Krizaj, 2019). IOP-lowering strategies have been limited to reducing production of aqueous humor in the ciliary body and/or facilitation of aqueous outflow across the ciliary muscle. Treatments to enhance outflow across the trabecular meshwork (TM), the mechanosensitive tissue that mediates 80-90% of aqueous outflow have been lacking until the recent approval of Rho kinase inhibitors which suppress IOP-dependent polymerization of TM actin cytoskeleton (Rao et al., 2017). Such treatments are not always effective and there are significant side effects (Sakamoto et al., 2019). Thus, there is a significant unmet need to control IOP through facilitation of the trabecular outflow pathway.

An intuitively obvious target for glaucoma therapies are mechanotransduction pathways within the TM cells themselves. The mechanotransduction properties of TM cells ensure that aqueous outflow matches production in order to protect vision from mechanical injury by increasing the outflow of aqueous humor (Bradley et al., 2001). Additional mechanosensitive mechanisms regulate the rhythmic IOP fluctuations and control the outflow pathway in response to rapid IOP elevations induced by stressful situations (Turner et al., 2019). Excessive mechanotransducer activation leads to pathological actin polymerization, increased cell contractility and stiffness that epitomize glaucomatous TM remodeling (Last et al., 2011; Vahabikashi et al., 2019) yet despite their physiological and translational significance, neither the identity of TM pressure sensors nor their function are currently understood. A potentially suitable feedback regulator of trabecular outflow could be shear impelled by aqueous flow yet it is not known whether shear stress within the TM (~0.05 dyn/cm$^2$) is sufficient to stimulate the endogenous mechanosensing mechanisms (Sherwood et al., 2019; McDonnell et al., 2020).

Calcium influx through stretch-activated Piezo and TRP (transient receptor potential) ion channels plays fundamental functions in pressure homeostasis in vasculature, lung and bladder tissues (Xia et al., 2013; Ranade et al., 2015; Retailleau et al., 2015; Ryskamp et al., 2016). Piezo channels have recently been implicated in dynamic regulation of pressure-induced lung vascular hyperpermeability and shear-stress induced endothelial signaling (Friedrich et al., 2019; Iring et al., 2019). Piezo 1 and 2 are large, conserved trimeric channels that mediate rapidly inactivating, small conductance (~25 - 35 pS), low-threshold (~0.6 kBT/nm$^2$) currents in response to membrane tension (~1 - 3 mN/m), indentation, shear stress (~10 dyn/cm$^2$) and/or stretch (Coste et al., 2010; Kim et al., 2012; Rode et al., 2017; Del Marmol et al., 2018). The Genotype-Tissue Expression (GTEx) project (Lonsdale et al., 2013) shows Piezo1 expression in nonexcitable cells from multiple pressure regulating tissues. While the channel plays a central role in smooth muscle cell (SMC)- and endothelial regulation of cell volume, heart rate and flow-mediated vasoconstriction (Li et al., 2015; Murthy et al., 2017; Albarran-Juarez et al., 2018; Zeng et al., 2018; Douguet & Honore, 2019), it is not known if it has functions in ocular tissues. Another potential regulator of pressure sensing is the polymodal nonselective cation channel TRPV4, which promotes

calcium increases, cytoskeletal polymerization, cell stiffening (Adapala et al., 2013; Ryskamp et al., 2016; Sharma et al., 2019) and ECM assembly (Gilchrist et al., 2019; Lakk & Krizaj, 2020) that underlie function, pathology and repair in load-bearing tissues. TRPV4 activation stimulates Rho signaling, actin and fibronectin expression and suppresses fluid flow in an *in vitro* model of trabecular outflow (Ryskamp et al., 2016; Lakk & Krizaj, 2020) but its responsiveness to pressure stimuli has been controversial (Lu et al., 2014; Servin-Vences et al., 2017; Yarishkin et al., 2018; Sherwood et al., 2019).

The objective of this study was to define the TM mechanosensors and link them to architectural remodeling that drives the increase in trabecular outflow resistance in glaucoma. We identify Piezo1 as a principal transducer of membrane tension and shear flow in human TM cells and link its activation to dynamic control of the TM cytoskeleton, cell-ECM contacts and aqueous outflow. Inhibition of Piezo1 resulted in striking suppression of trabecular outflow, suggesting that dynamic stimulation of the channel protects the eye from glaucoma in the presence of IOP stress. Furthermore, we show that pressure stimuli evoke a delayed component of the stretch-activated current that is mediated by TRPV4 channels. By demonstrating that TM mechanotransduction involves contributions from kinetically and pharmacologically distinguishable SACs, this study identifies potential targets for novel IOP -lowering strategies in the treatment of glaucoma.

## Methods

### Ethical Approval.

We acknowledge the ethical principles of *The Journal of Physiology*, and confirm our animal procedures were performed within these principles as well as in accordance with the NIH Guide for the Care and Use of Laboratory Animals, the ARVO Statement for the Use of Animals in Ophthalmic and Vision Research, and the Institutional Animal Care and Use Committees at the University of Utah and Duke University (IACUC approval 19-04005 and A184-18-08, respectively).

### TM cell culture and transfection.

All procedures and protocols conformed to the standards set by the WMA Declaration of Helsinki and the Department of Health and Human Services Belmont Report, and complied with the ethics policies of the Journal of Physiology. De-identified postmortem eyes from two donors (65 year-old male, 78 year-old female). with no history of glaucoma were procured from Utah Lions Eye Bank with written informed consent of the donors' families. The maximum processing time was 3.5-4 hours. TM cells were isolated from juxtacanalicular and corneoscleral regions, as previously described (Ryskamp et al., 2016; Yarishkin et al., 2018), in accordance with consensus characterization recommendations (Keller et al., 2018). Passage 2 – 6 cells were seeded onto Collagen I-seeded coverslips and grown in Trabecular Meshwork Cell Medium (ScienCell, Catalog#6591) at 37°C and 5% $CO_2$. Vehicle control scrambled shRNA (Sc-shRNA; Cat#: TR30021) and human Piezo1 shRNA (Cat#: TF313084) were purchased from OriGene. Cells were transiently transfected with shRNA constructs (5 μg per 25 $cm^2$ tissue culture flask) using Lipofectamin 3000 reagent and utilized for experiments on $3^{rd}$-$4^{th}$ day post-transfection. Transfected cells were

recognized by expression of the fluorescent reporter (GFP and mCherry for Sc-shRNA and Piezo1 shRNA, respectively).

### Animals.

C57BL/6J and *Piezo1*$^{P1\text{-}tdT}$ (*Piezo1*$^{tm1.1Apat}$) mice were from JAX (#02914; Bar Harbor, ME). The initial transgenic 129/SvJ strain (Ranade et al., 2014) was backcrossed to C57BL/6J for more than 8 generations. The animals were maintained in a pathogen-free facility with a 12-hour light/dark cycle and *ad libitum* access to food and water. Temperature was set at ~22-23°C. No sex differences in the immunolabeling data were noted, so their data were pooled. Mice were 3 to 6 months in age.

### Reagents.

Reagents used were largely purchased from Sigma-Aldrich. 2-[5-[[(2,6-Dichlorophenyl)methyl]thio]-1,3,4-thiadiazol-2-yl]-pyrazine (Yoda1) and *Grammostola spatulata* mechanotoxin 4 (GsMTx4) were from Sigma-Aldrich and Alomone Labs, respectively.

### RT-PCR.

Total RNA was extracted from TM cells using Applied Biosystems PicoPure RNA Isolation Kit (ThermoFisher Scientific) (Phuong et al., 2017). 1 μg of total RNA was used for complementary DNA synthesis. RNA was reverse transcribed using qScript XLT cDNA Supermix (Quanta Biosciences). PCR was performed using Apex qPCR 2x Master Mix (Genesee Scientific) with Applied Biosystems Veriti Thermal Cycler (ThermoFisher Scientific). PCR conditions were as follows: 95°C for 15min; 95°C for 20s, 60°C for 60s, 40 cycles. PCR products were run on a 2% agarose gel at 90V for 30min. The DNA bands were visualized by Ethidium Bromide staining along with 100-bp DNA ladder (IBI Scientific) using a FluorChemQ gel imaging system (Cell Biosciences).

### Immunohistochemistry.

C57BL/6J and *Piezo1*$^{P1\text{-}tdT}$ (*Piezo1*$^{tm1.1Apat}$) mice were killed by isoflurane inhalation followed by cervical dislocation, after which eyes were enucleated. Anterior chambers were fixed in 4% para-formaldehyde for one hour, cryoprotected in 15 and 30% sucrose gradients, embedded in Tissue-Tek® O.C.T. (Sakura, 4583), and cryosectioned at 12 μm, as described (Jo et al., 2017; Lakk et al., 2018). The sections were probed with antibodies against Piezo1 (Proteintech, 15939), α-SMA (Sigma, A2457), and Collagen IV (EMD Millipore, AB769). Secondary antibodies included anti-rabbit IgG DyLight 488 (Invitrogen, 35552), anti-mouse IgG DyLight 594 (Invitrogen, 35511), and anti-goat IgG Alexa 647 (Invitrogen, A21469). Sections were coverslipped with DAPI-Fluoromount-G (EMS, 17984-24) and imaged with Fluoview-1000 confocal microscope (Olympus, Center Valley, PA).

### Calcium imaging.

TM cells were seeded on glass coverslip for 48 h, loaded with Fura-2AM (Invitrogen) for 40-60 min, and washed with the bath solution containing (in mM): 140 NaCl, 2.5 KCl, 1.2 $MgCl_2$, 5.6 glucose, 10 HEPES, 1.8 $CaCl_2$ (pH 7.4, osmolarity 295 – 300 mOsm) for 5 - 30

min. Fluorescent imaging followed published protocols (Ryskamp et al., 2014; Molnar et al., 2016). Excitation for 340 nm and 380 nm filters (Semrock, Rochester, NY) was delivered by a liquid light guide from a 150W Xenon arc lamp (DG-4, Sutter Instruments). Fluorescence emission was high pass-filtered at 510 nm and captured with a cooled digital CCD camera (Photometrics) binned at 2×2. Data acquisition, $F_{340}/F_{380}$ ratio calculations and background subtraction were performed by NIS Elements 3.22 (Nikon) on Regions of Interest (ROI) encompassing the central cell area. In cell poking experiments, cells were loaded with Fluo-4 AM for 50 min at 37°C in $CO_2/O_2$ incubator. Poking of cells is described below. For data analysis, Fluo-4 fluorescence was normalized to mean baseline values obtained prior to poking. All imaging experiments were performed at room temperature (20 – 22°C).

### Electrophysiology.

Borosilicate patch pipettes (WPI) were pulled using a P-1000 micropipette puller (Sutter Instruments), with resistance 6-8 MΩ when filled with the internal buffer solution containing (mM): 125 K-gluconate, 10 KCl, 1.5 $MgCl_2$, 10 HEPES, 10 EGTA, pH 7.4. The chamber was superfused with saline containing (in mM): 140 NaCl, 2.5 KCl, 1.5 $MgCl_2$, 1.5 $CaCl_2$, 5.6 D-glucose, 10 HEPES (pH 7.4, adjusted with NaOH)(Yarishkin et al., 2018; Yarishkin et al., 2019). In some experiments $K^+$ in bathing and pipette solutions was replaced with equimolar concentration of $Na^+$. The bathing solution for patch clamp experiments combined with whole-cell High-Speed Pressure Clamp contained 100 μM 4,4-Diisothiocyanatostilbene disulfonic acid (DIDS). The holding potential in the whole-cell recordings was set to −40 mV. In some voltage-clamp experiments, the holding potential was set to −100 mV to minimize contribution of TREK-1 channels (Yarishkin et al., 2018).

The bathing solution for excised (inside-out) patch clamp experiments contained (mM): 140 NaCl, 2.5 KCl, 1.5 $MgCl_2$, 10 ethylene glycol-bis(β-aminoethyl ether)-N,N,N’,N”-tetraacetic acid (EGTA), 5.6 D-glucose, 10 HEPES (pH 7.4, adjusted with NaOH). The pipette solution used in excised patch recordings contained 140 NaCl, 2.5 KCl, 1.5 $MgCl_2$, 1.5 $CaCl_2$, 5.6 D-glucose, 10 HEPES (pH 7.4, adjusted with NaOH). The membrane capacitance of TM cells was measured using pClamp 10.6 software (Molecular Devices) and was 51.46 ± 35.36 pF (n = 166 cells). Patch clamp data was acquired with a Multiclamp 700B amplifier, pClamp 10.6 software and Digidata 1440A interface (all from Molecular Devices). Data was sampled at 5 kH and 10 kHz for whole-cell and excised patch recording, respectively, digitized at 2 kH and 5 kHz for whole-cell and excised patch recording, respectively, and analyzed with Clampfit 10.7 (Molecular Devices) and Origin 8 Pro (OriginLab).

Steps of positive (in whole-cell recording) and negative (in single-channel recording) pressure were delivered via High-Speed Pressure Clamp (ALA Scientific) as described (Fig. 1A) (Yarishkin et al., 2018; Yarishkin et al., 2019). In some experiments, membrane stretch caused by pressure application was visualized as increased fluorescence of the cell volume marker calcein (Fig. 1B and C) (Toft-Bertelsen et al., 2019). The timing and intensity of pressure steps were controlled by Clampex software. To minimize membrane creep, membrane potential rundown and/or desensitization/inactivation (Coste et al., 2010; Gottlieb et al., 2012) a single stimulus was executed per cell in the whole-cell recording and two

stimuli were applied to the excised patch. Single channel stimuli were −80 mm Hg and 500 msec duration, whole cell stimuli were −25 mm Hg and 1.5 sec duration. The single channel conductance was computed using linear fitting through the current-voltage relationship plots. Single channel amplitude histograms were fitted with Gaussian equation. Current-voltage (I-V) relationship of Yoda1-induced whole-cell current were obtained from voltage Ramps ascending from the holding potential −100 mV to 100 mV (200 mV/sec). Histograms of unitary current amplitude were fitted with a Gaussian distribution using OriginPro 2020b (OriginLab). Non-linear optimization was done using the Levenberg-Marquardt algorithm.

Indentation responses were elicited with a glass pipette (tip diameter ~ 3 μm) position at a 30° angle relative to the cover glass. The probe was positioned ~ 2 μm from the cell using a Sutter MPC-200 micromanipulator and indented with a rapid manual step to the depth of ~ 60 nm for 1 sec.

All patch clamp experiments were performed at room temperature (20 – 22°C).

### Shear flow.

Shear stress-induced changes in intracellular calcium were tracked in a microfluidic chamber designed for laminar flow, precise control of shear and full access to microscope objectives (Warner Instruments). TM cells were plated on type I collagen coated glass coverslips 48 hours before being loaded into the shear flow chamber for experiments to prevent cell detachment due to shear flow. A programmable peristaltic pump (Harvard Apparatus) was used to control the total media flow rate, with shear Stress calculated using the following equation:

$$\gamma = V / x \text{ and } \tau = \gamma^{*}\eta$$

with shear rate, $\gamma$, velocity of the moving layer, V, and distance between layers, x, shear stress, $\tau$, and viscosity, $\eta$. $\gamma$ experienced by cells in the chamber was estimated as 0.5 dyn/cm$^2$. Fluorescence imaging was conducted with an inverted Nikon Eclipse Ti microscope using a 40x objective.

For immunocytochemistry experiments, cells were shear-stressed (0.5 dyn/cm$^2$) for 1 h min prior to fixation in PFA.

### Immunocytochemistry and imaging.

Antibody staining and analysis followed the protocols outlined in (Lakk & Krizaj, 2020). TM cells were plated on type I collagen coated glass coverslips for 48 h before undergoing treatment with Yoda1, GsMTx4 or vehicle for 1 hour at 37°C in cell culture $CO_2/O_2$ incubator. Cells were fixed in 4% PFA, washed in PBS, permeabilized with 0.1% Triton X-100, and exposed to the blocking solution (1% BSA, 0.3% Triton X-100/PBS) (Ryskamp et al., 2016). Slides were probed with antibodies raised against vinculin (1:1000; Sigma). Secondary antibodies were anti-mouse IgG Alexa Fluor 647 (1:1000; Invitrogen) or anti-mouse IgG Alexa Fluor 488 (1:1000; Invitrogen) for Yoda1-treated cells and shear-stressed cells, respectively. DAPI-Fluoromount-G-coverslipped slides were imaged with a Fluoview-

CV1200 confocal microscope (Olympus, Center Valley, PA). Images were processed with Photoshop CS6 (Adobe, San Jose, CA).

### Outflow Facility Measurements.

C57BL/6 mice (2 males and 6 females, 3-6 months old) were euthanized by isoflurane inhalation followed by decapitation. Eyes were immediately enucleated and used for experimental procedures. Each eye of pair was attached to a support platform in one of two identical perfusion chambers using a small amount of cyanoacrylate glue (Loctite, Westlake Ohio, USA). The perfusion chamber was filled with pre-warmed phosphate-buffered saline containing 5.5mM glucose and divalent cations (DBG), and temperature was maintained at 35°C. A glass microneedle was filled with DBG containing 6 μM GsMTx4 (Alomone Labs, Jerusalem, Israel) or DBG alone. The microneedle was connected to the perfusion system and was inserted into anterior chamber using a micromanipulator, while visualized under a stereomicroscope. Outflow facility was measured using the iPerfusion system, which is specifically designed to measure the low flow rates in the outflow system of paired mouse eyes (Sherwood et al., 2016). Initially, both eyes were perfused at 12 mmHg for 60 min to allow acclimation and delivery of the drug to cells of the outflow pathway, followed by 9 sequential pressure steps, with equal intervals between 5 and 17 mmHg. Data analysis was carried out as described previously (Sherwood et al., 2016). Briefly, a non-linear flow-pressure model was used to account for the pressure dependence of outflow facility in mice. Outflow facility (C) was calculated as flow (Q) divided by pressure (P), as represented by the bottom right panel of figure 13A. The exponent β characterizes the nonlinearity of the flow-pressure relationship, or outflow facility. A reference pressure of 8 mm Hg was used to calculate the outflow facility. The order (left versus right and drug versus control) in which eye perfusions were performed was randomized.

### Data analysis.

Student's paired *t*-test, two-sample *t*-test or ANOVA multiple comparisons test were applied to estimate statistical significance of results. $P < 0.05$ was considered statistically significant. Results are presented as the mean ± SD. The data that support the findings of this study are available from the corresponding author upon reasonable request.

## Results

### SAC activity in TM cells involves kinetically separable components.

We investigated mechanotransduction in primary TM cells isolated from two healthy donors. The cells expressed standard TM markers, including *MYOC, TIM3, AQP1, MGP* and *ACTA2* and responded to steroid DEX with MYOC upregulation (Fig. 5A and (Yarishkin et al., 2019)). Stretch-activated currents were measured under voltage clamp in the whole-cell configuration, at the holding potential of −40 mV that approximates the cells' resting potential (Yarishkin et al., 2018). The cell membrane was expanded by application of hydrostatic pressure (1.5 sec, 25 mm Hg) delivered by high-speed pressure clamp (HSPC) (Fig. 1A - C), a method that has been widely used to study SAC activation (Besch et al., 2002; Cox et al., 2016; Lewis et al., 2017). Application of pressure steps evoked transmembrane current in the majority (55/57 cells; 96%) of recorded cells. A rapidly-

activated current (referred to as the “fast component”), seen in 72% of cells (n = 41/57 cells), showed an average amplitude of −76.1 ± 43.6 pA/pF (mean ± S.E.M.) The pressure response reached peak amplitude within 1.18 ± 0.50 sec (Fig. 1D - F).

In a large subpopulation of cells we observed kinetically different pressure-evoked transmembrane current (Fig. 1D - F). This type of the response to pressure (further referred to as the “slow component”) was characterized by delayed onset (peak response latency of 113 ± 8 sec), and slow return towards the baseline conductance. The average maximal amplitude of the “slow component” was −3.7 ± 3.1 pA/pF (n = 9 cells). This component was observed in 45% cells including ~14 % of cells exhibiting both components. These data demonstrate that TM cells isolated from healthy donors consist of functional subpopulations that differ by the kinetics of nonselective cation SAC conductance.

### Piezo1 mediates fast and TRPV4 mediates slow SAC activation in human TM cells.

We investigated whether the time-dependence of the pressure-induced response involves distinct SACs. To identify the ion channel mediating the fast component, pressure steps were applied in the presence of Ruthenium Red (RR; 10 μM), a nonselective polycationic inhibitor of calcium-permeable mechanochannels. RR inhibited the fast component by 77 % (n = 7 cells) whereas HC067047 (5 μM), a selective blocker of TRPV4 channels had no effect (n = 15 cells). However, pretreatment with the *Grammostola spatulata* mechanotoxin GsMTx4 (5 μM), a relatively selective extracellular blocker of the Piezo family (Bae et al., 2011; Gottlieb & Sachs, 2012), attenuated the fast component from −76.1 ± 37.0 pA/pF to −19.6 ± 21.5 pA/pF (~86 %; n = 15 cells) (Fig. 2A-C). Piezo1 involvement was tested more precisely in cells overexpressing a Piezo1 shRNA construct that demonstrated 50-60% knockdown relative to scrambled Sc-shRNA (Fig. 2D). The pressure response in in Sc-shRNA-transfected controls (−51.4 ± 19.9 pA/pF; n = 4 cells) was attenuated from to −5.5 ± 11.0 pA/pF (n = 4 cells) following treatment with Piezo1 shRNA, a ~85% decrease (Fig. 2E and F).

To gain insight into channel kinetics, we measured single channel currents in excised (inside-out) patches of the TM membrane (Fig. 3A). Pressure steps (−80 mm Hg) induced single channel activity in 12/36 patches (Fig. 3B and C). In agreement with the reported conductance of human Piezo1 (Li et al., 2015), the amplitude of the average unitary current measured at the membrane potential −100 mV was 2.15 ± 0.14 pA (n = 7 patches; Fig. 3B). Due to brief bursts of activity and prolonged inactivation of the Piezo1-like channel we were unable to reconstruct its I-V relationship. To confirm the activity of Piezo1 channel in the TM plasma membrane, we characterized the single channel current activated by a selective Piezo1 agonist Yoda1. Application of Yoda1 from the cytosolic side of the excised membrane patch triggered the activity of single or multiple channels in the patch (Fig. 3E and H). The amplitude of the channel measured at the membrane potential of −100 mV was −2.32 ± 0.16 pA, which was almost identical to the Piezo1-like channel activated by the pressure pulse (Fig. 3F and G). The Yoda1-induced channel had slightly inwardly rectifying I-V relationship with the slope conductance ≈27 pS and ≈19 pS at negative and positive membrane potentials, respectively (Fig. 3H and I). In accordance with these data, mechanosensitive 2.15 pA events were not observed in patches from cells overexpressing

Piezo1 shRNA (0/27 patches) whereas Sc-shRNA-treated cells showed channel activity in 13/35 patches (Fig. 3J and K).

To get a more precise estimate of the time course of the fast component, we evaluated the latency of the indentation response (Coste et al., 2010; Brohawn et al., 2014). Poking cells with a glass probe evoked robust inward currents with the activation and inactivation kinetics of 1.1 ± 0.4 ms and 1.8 ± 0.8 ms, respectively (Fig. 4A-C). The time course of the fast response indicates that the channel is directly activated by lipid distension (Lewis & Grandl, 2015; Syeda et al., 2016; Cox & Gottlieb, 2019). GsMtx4 suppressed 71.1 % of the poke-induced current (Fig. 4C). These results suggest that the fast response to the pressure step is largely mediated by Piezo1.

Since Piezo1 is known to mediate a non-selective cation transmembrane conductance, we tested effects of the fast component of the pressure response on the plasma membrane potential. We found that the pressure pulse results in transient depolarization of the plasma membrane from −27.4 ± 10.3 mV to 12.6 ± 1.3 mV (Fig. 5A and B). Interestingly, this depolarization was followed by more sustained hyperpolarizing shift to −32.4 ± 4.5 mV from −21.8 ± 4.7 mV in ~50 % of cells (Fig. 5A and C). This sustained hyperpolarizing response was also observed in a subpopulation of cells that did not demonstrate the fast component in the response to pressure. We previously showed that the same pressure clamp protocols activate mechanosensitive TREK-1 potassium channels (Yarishkin et al., 2018). It remains to be seen whether the hyperpolarization that follows Piezo1/TRPV4 activation (Fig. 5C) involves concomitant TREK-1 signaling and/or activation of high-conductance $Ca^{2+}$-activated $K^+$ (BK) channels (Gasull et al., 2003).

To address biophysical properties of the slow component more precisely, we performed whole-cell current recording in $K^+$-free extracellular and pipette solutions. Under these experimental conditions, the pressure pulse evoked a slowly developing robust transmembrane current that had an outwardly rectifying I-V relationship (Fig. 5D and E). The current reached the amplitude −22.4 ± 15.3 pA and 32.9 ± 8.3 pA/pF at −100 mV and 100 mV, respectively, and had the reversal potential of 6.0 ± 4.4 mV (Fig. 5F). These results suggest that the current is mediated by a cation permeability pathway of ion conductance.

Given that TRPV4 is expressed in mouse and human TM, is activated by membrane strain and may modulate the outflow facility (Ryskamp et al., 2016; Yarishkin et al., 2018), we wondered whether it contributes to the slow component of the pressure response. At the holding potential of −100 mV (aimed to minimize contamination of the slow response with $K^+$ conductance), pressure steps evoked a robust, slowly-developing negative current in 8 out of 9 cells (−12.5 ± 5.9 pA/pF, n = 8 cells) that was sensitive to a selective TRPV4 antagonist HC067047. The antagonist attenuated the peak current to −4.1 ± 3.6 pA/pF (n = 8 cells), with an average suppression of ≈73 % (Fig. 5G & H). Thus, SAC transduction in TM cells involves kinetically and functionally distinct Piezo1 and TRPV4 components.

### Molecular characterization of Piezo1 expression.

To gain insight into the relative expression and localization of SACs, we used RT-PCR and immunohistochemistry in TM cells expressing the standard markers αSMA, AQP1 and

MYOC. mRNAs encoding Piezo1, Piezo2 and TRPV4 were detected (Fig. 6A). The anti-Piezo1 antibody labeled isolated cells, intact human TM and mouse TM tissue, with cultured cells showing cytosolic and membrane signals (Fig. 6B). This immunoreactivity pattern might reflect multiple Piezo1 pools (e.g., the plasma membrane, trafficked pools as well as proteins undergoing posttranslational modifications). Anterior segments isolated from normotensive donors showed prominent Piezo1-ir, which colocalized with TM markers α-SMA, collagen IV (Fig. 6C) and aquaporin 1 (not shown). Piezo1 localization to inflow and outflow pathways indicates that it is well placed to participate actively as a sensor of pressure-induced changes. Similar to human, Piezo1 was robustly expressed in TM in normotensive mice, with the signal observed in the TM, the ciliary body and cornea (Fig. 6D). In addition, Piezo1 expression was observed in nonpigmented cells of the ciliary body, ciliary muscle, stromal keratinocytes, and corneal epithelial cells. To validate antibody labeling, we examined Piezo1 expression in TM from $Piezo1^{P1\text{-}tdT}$ mice, which express the fluorescent reporter (*td*Tomato) that was inserted in front of the Piezo1 stop codon in exon 51 (Ranade et al., 2014). Fig. 6E shows prominent signal within the TM, the ciliary body and cornea.

### Piezo1 mediates nonselective cation influx and increase in $[Ca^{2+}]_i$.

To verify that TM cells respond with Piezo1 activation in the absence of mechanical stressors, we assessed the response to the gating modifier Yoda1, which binds the C-terminal Agonist Transduction Motif (ATM) to stabilize the open pore (Syeda et al., 2015; Lacroix et al., 2018). Voltage-clamped cells responded to Yoda1 with an increase in the transmembrane current amplitude from −34.5 ± 23.3 pA at rest to −170.2 ± 118.7 pA and from 325.9 ± 222.2 pA at rest to 564.4 ± 340.8 pA measured at −100 mV and 100 mV, respectively (Fig. 7A-C). The current-voltage (I-V) relationship of the whole-cell current was outwardly rectifying (Fig. 7D), showing a 32.6 ± 16.0 mV shift of the reversal potential to the positive direction. The Yoda1-induced current showed no detectable inactivation in continued presence of the activator and it deactivated at negative membrane potentials, but deactivation was rarely observed at positive potentials (Fig. 7A). The outward rectification of the Yoda1-induced current are consistent with reported the properties of the Piezo1-mediated current (Wu et al., 2017; Moroni et al., 2018). Analysis of Yoda1-induced changes in membrane potential showed a transient hyperpolarizing component peak followed by sustained depolarization from the resting potential −47.3 ± 12.1 mV to −1.7 ± 6.2 mV (Fig. 7E and F). The Yoda1-induced depolarization appears more sustained than depolarization evoked by the pressure pulse step, which might reflect the modulation of the Piezo1 activity by the agonist that was reported to increase the open probability of the channel (Lacroix et al., 2018; Qiu et al., 2019). We assessed the spatial and temporal properties of Yoda1-induced $Ca^{2+}$ signals, which might reflect the Piezo1 potential for regulating downstream signaling. The activator induced robust elevations in $[Ca^{2+}]_i$ across the TM cell (Fig. 8A & C), which were abrogated by ≈ 99 % during the removal of extracellular $Ca^{2+}$ (Fig. 8B & C). Ruthenium Red reduced Yoda1-evoked $[Ca^{2+}]_i$ signals by ≈ 68 % (Fig. 7D & E) whereas GsMTx4 evinced ~73 % inhibition (n = 17/15 for untreated control and GsMTx4-treated cells, respectively) (Fig. 8F & G). Piezo1 knockdown with shRNA inhibited Yoda1-induced $[Ca^{2+}]_i$ signals by ~50% (n = 25 and 17 cells for Sc and Piezo1 shRNA-treated cells, respectively) (Fig. 8H & I).

Mechanical stimulation by cell poking with the glass probe induced a robust elevation of $[Ca^{2+}]_i$ (296.9 % relative to baseline levels). This effect was inhibited by GsMTx4 by 33 % (Fig. 9), indicating that the $Ca^{2+}$ signals in TM cells are mediated by the mechanosensitive Piezo1 channel.

### Piezo1 is critically required for shear flow-induced TM $[Ca^{2+}]_i$ response.

The bulk flow of aqueous humor driven by the pressure gradient imposes a drag force (shear) on the TM, particularly in the narrow passage ways of the JCT with predicted shears of 0.5 – 2 dynes/cm$^2$ (WuDunn, 2009). To test whether TM cells are capable of responding to shear forces that mirror those encountered *in situ*, ratiometric Fura-2 calcium signals were measured in cells placed in a microfluidic chamber designed for laminar flow. The flow rate of 130 μL/min was applied through our shear chamber to produce a physiological shear stress of 0.5 dyn/cm$^2$ (Sherwood et al., 2019). Exposure to shear elevated $[Ca^{2+}]_i$ from baseline to the peak level of 0.714 ± 0.518 (n = 77 cells), following which $[Ca^{2+}]_i$ recovered to a steady plateau. GsMTx4 reduced response amplitude by 83.1 % (Fig. 10B & C), Ruthenium Red suppressed shear-evoked $[Ca^{2+}]_i$ signals by ~72.5 % whereas the TRPV4 antagonist HC067047 exerted only a slight inhibitory effect (7.1 %) (Fig. 10B & C). These results identify Piezo1 as the principal transducer of shear flow in the TM.

### Activation of Piezo1 upregulates focal adhesions in TM cells.

Cell-ECM contacts contribute to TM stiffness and rigidity, and were suggested to represent an important determinant of mechanically induced outflow of aqueous humor (Filla et al., 2017; Faralli et al., 2020). To test the hypothesis that Piezo1 activation is sufficient to regulate focal contacts, we investigated Yoda1-dependence of vinculin, a principal component of the focal complex. Exposure to Yoda1 (30 min, 2 μM and 10 μM) significantly increased the number of vinculin-immunoreactivity (ir) puncta (by 41.2 and 62.8 % by 2 μM and 10 μM of Yoda1, respectively) without altering the cell area (Fig. 11). Likewise, shear stress significantly increased the number of vinculin-ir sites in a manner that was sensitive to GsMtx4 (Fig. 12). These results suggest that shear stress might modulate the dynamic reorganization of cell-ECM contacts through stimulation of Piezo1 channels.

### Effect of Piezo1 blockade on outflow facility.

We sought to determine whether Piezo1 activity is a component of pressure-induced regulation of TM-mediated hydraulic conductivity (“outflow facility”). Flow rate in response to sequential pressure steps was measured pairwise in enucleated mouse eyes, in the presence or absence of GsMTx4 (6 μM). The antagonist significantly reduced outflow facility (3.1 ± 0.8 nl/min/mmHg) as compared to control (4.6 ± 1.3 nl/min/mmHg) (Fig. 13), a 33% reduction. These data suggest that Piezo1 activity significantly augments fluid drainage via the pressure-regulated conventional outflow pathway.

## Discussion

In this study, we demonstrate that Piezo1 is required for the TM transduction of shear flow and membrane stretch, and link its activation to flow-induced focal adhesion remodeling. Piezo1 sensitivity to weak hydrodynamic loading, rapid activation, and role in cell-ECM

signaling support a model whereby the channel stabilizes and fine-tunes the outflow resistance in response to acute IOP displacements. Another, delayed SAC component was mediated by TRPV4 channels, which may collaborate with Piezo1 channels to impart mechanosensitivity to the ocular outflow system. The expression, sequence homology (Lonsdale et al., 2013) and similar functional properties of Piezo1 in mouse and human TM suggest that its role in outflow regulation may be conserved across mammals.

It has long been obvious that the visual system is protected from pressure-induced neuropathy by sophisticated mechanotransduction mechanisms in the TM (Bradley et al., 2001; Sherwood et al., 2019). Putative mechanotransducers in TM cells include Piezo1 (Tran et al., 2014), TREK-1 (Carreon et al., 2017; Yarishkin et al., 2018), TRPV4 channels (Luo et al., 2014; Ryskamp et al., 2016), primary cilia (Luo et al., 2012), glycocalyx-actin interactions (Acott et al., 2014) and integrin-based cell-ECM adhesions (Faralli et al., 2019; Faralli et al., 2020). Similar to SMCs and vascular endothelial cells (Ranade et al., 2014; Retailleau et al., 2015), TM cells expressed high transcript levels of Piezo1 and TRPV4. Double labeling with JCT-selective marker (αSMA) and analysis of *td*Tomato fluorescence from transgenic *Piezo1*$^{tm1.1Apat}$ retinas confirmed Piezo1 expression in mouse and human TM. Accordingly, Yoda1, which stimulates Piezo1 but not Piezo2 (Syeda et al., 2015; Lacroix et al., 2018), evoked robust increases in $[Ca^{2+}]_{TM}$. Functional analyses that employed poking and pressure pulse steps revealed mechanosensitive current with single channel amplitude of ~2.2 pA and fast activation and inactivation kinetics. Indicating that Piezo1 is required for TM mechanotransduction, the current was inhibited by Ruthenium Red, GsMTx4 and attenuated in Piezo1-deficient cells. These findings are consistent with its functions in vascular pressure regulation and inflammatory mechanosensation (Li et al., 2014; Douguet & Honore, 2019; Solis et al., 2019).

In general, the levels of shear stress across the TM are thought to be negligible, except for the JCT region that may experience ~0.5 – 2 dyn/cm$^2$ and the Schlemm's canal, where shear may reach up to 30 dyn/cm$^2$ (Sherwood et al., 2019; McDonnell et al., 2020). It has long been unclear whether shear stress constitutes a physiologically relevant stimulus for the TM (e.g., (Sherwood et al., 2019; McDonnell et al., 2020). Our discovery that shear flows 1-2 orders of magnitude lower compared to stresses typically used to stimulate endothelial and Piezo1-transfected HEK-293 cells (Li et al., 2014; Ranade et al., 2014; Rode et al., 2017) reliably produce calcium responses suggests that aqueous hydrodynamics might be sufficient to regulate intracellular signaling in response to small IOP fluctuations that impose shear on juxtacanalicular cells (Johnstone, 2004; Sherwood et al., 2019). The sensitivity of flow-induced signals to GsMTx4 and Piezo1 knockdown identifies Piezo1 as the principal transducer of these responses. The fraction (~7%) of the flow-induced signal that was mediated by TRPV4 is in line with reports of TRPV4-dependent shear transduction in SMCs and endothelia (Kohler & Hoyer, 2007; Thodeti et al., 2009; Corrigan et al., 2018; Swain et al., 2020) but it remains to be seen whether the TRPV4 component is increased by shear stresses induced by larger pressure gradients (Kohler & Hoyer, 2007; Thodeti et al., 2009; Corrigan et al., 2018).

Trabecular outflow is the principal IOP-regulating mechanism in rodent and primate eyes. The ~30% reduction in pressure-dependent fluid outflow observed in GsMTx4-treated eyes

(Fig. 13) suggests the possibility that Piezo1 activation resets the increase in pressure drop across the juxtacanalicular TM. The effect of the Piezo1 antagonist, which functions as an amphipathic channel blocker by lowering lipid strain on the channels (Suchyna et al., 2004) was comparable to glucocorticoids and TGF$\beta$2, known drivers of ocular hypertension in glaucoma that reduce outflow facility by 23 – 46% (Kumar et al., 2013; Patel et al., 2017; Li et al., 2019) and 33%, respectively (Shepard et al., 2010). The millisecond onset of Piezo1 activation (Fig. 4) further suggests that Piezo1 provides rapid, homeostatic adjustments to increments in pressure.

Excessive actin polymerization, αSMA-dependent contractility and ECM upregulation represent key harbingers of increased outflow resistance in glaucoma (Peterson et al., 1999; Rao et al., 2017). Indicating that mechanotransduction contributes to use-dependent formation, alignment and plasticity of cell contacts, we found that exposure to Yoda1 suffices for the upregulation of vinculin-containing focal puncta. Similar results were observed in cells stimulated with TRPV4 agonists and pressure (Ryskamp et al., 2016; Lakk & Krizaj, 2020), pointing at calcium as the likely mediator of mechanically induced remodeling of actomyosin and cell-ECM contacts. We propose that mechanosensitive Piezo1 and TRPV4 channels function as transducers of mechanical stresses within the local hydromechanical milieu within the anterior eye that regulate of calcium- and use-dependent pathways associated with TM contractility and remodeling. Taking into account the mechanosensitive TREK-1 channels that may counterbalance pressure-dependent cation fluxes through Piezo1 and TRPV4 (Brohawn et al., 2014; Yarishkin et al., 2018), these data suggest that pressure homeostasis within the TM outflow involves at least three different channel-mediated mechanotransduction pathways. The prominent effect of GsMTx4 on the outflow facility measured with iPerfusion implicates Piezo1 in the dynamic regulation of the primary outflow pathway. Under our experimental conditions, outflow principally reflected the conventional pathway in which the JCT TM layer contributes ~75% of the outflow facility (Overby et al., 2009).

Pressure steps applied to whole cell-clamped cells evoked an additional, delayed, current component. This current, mediated by TRPV4 channels, was not detected in excised patch recordings, presumably due to the absence of eicosanoid intermediates that are necessary for channel activation (Watanabe et al., 2003; Ryskamp et al., 2016). Its manifestation in the absence of the fast component and resistance to GsMTx4 argue against Piezo1-TRPV4 coupling seen in pancreatic acinar cells (Swain et al., 2020). Interestingly, the tissue resistance to aqueous outflow is augmented in response to Piezo1 blockade, TRPV4 agonists and GPCR-coupled store release, all of which modulate cytosolic $[Ca^{2+}]_{TM}$ (Boussommier-Calleja et al., 2012). The following proof-of-principle examples suggest that functional divergence between $Ca^{2+}$ pathways in nonexcitable cells is not uncommon: (i) Piezo1 promotes vasoconstriction in mesenteric endothelia whereas TRPV4 channels drives vasodilation (Filosa et al., 2013; Rode et al., 2017); (ii) Piezo1-mediated depolarization in SMCs activates voltage-operated calcium influx and vasoconstriction whereas TRPV4 - mediates vasodilation (Beech & Kalli, 2019), and (iii) TRPV1 mediates contraction whereas TRPV4 mediates dilation of the ciliary muscle (Chen et al., 2019). We propose that Piezo1 and TRPV4 channels in TM cells are coupled to distinct microdomains and/or downstream $Ca^{2+}$ effectors.

TM mechanotransduction plays an essential role in IOP regulation and glaucoma. Here, we show that Piezo1 is one of the mechanosensors that initiates the response to hydrostatic pressure and is required for the rapid response to pressure, stretch and shear flow, with possible functions in the regulation of aqueous outflow. Such “high-pass” activation (Lewis & Grandl, 2015) might sense IOP fluctuations impelled by ocular pulse, blinking, sneezing or yoga (Turner et al., 2019) to modulate pulsatile flow of the aqueous fluid (Johnstone et al., 2011) and protect the eye through time-dependent facilitation of trabecular outflow. Our data suggest that Piezo1 collaborates with TRPV4, a stretch-activated channel that mediates cytoskeletal and cell-ECM remodeling in the presence of chronic mechanical stress (Ryskamp et al., 2016) however, the collaboration does not appear to require functional interaction between the channels. It is thus possible that mechanosensory tuning of outflow resistance under different pressure regimens, segmental flows of aqueous humor, and tensile strains on trabecular lamellae, involves concurrent and balanced activations of multiple mechanosensitive channels that include Piezo1, TRPV4 and TREK-1 (Ranade et al., 2015; Ryskamp et al., 2016; Krizaj, 2019). Also, worth noting are the many parallels with cardiovascular and pulmonary systems in which mechanochannel activation by fluid flow profoundly regulates hydrostatic pressure gradients associated with tissue development, function and pathology (Kim et al., 2016; Murthy et al., 2017; Soni et al., 2017; Zeng et al., 2018; Douguet & Honore, 2019). The delineation of the intertwined mechanisms that mediate the TM sensitivity to mechanical stress may help identify novel potential targets that can be exploited for precise IOP control and stabilization in glaucoma.

## Supplementary Material

Refer to Web version on PubMed Central for supplementary material.

## Acknowledgements

Supported by the National Institutes of Health (R01EY022076, P30EY014800, R01EY027920 to D.K.. T32EY024234 to C.N.R. and J.M.B., and R01EY022359, R01EY005722 to W.D.S.), Glaucoma Research Foundation, ALSAM-Skaggs Foundation, The Neuroscience Initiative at the University of Utah to D.K., and Unrestricted Grants from Research to Prevent Blindness to Departments of Ophthalmology at the University of Utah and Duke University.

## References

Acott TS, Kelley MJ, Keller KE, Vranka JA, Abu-Hassan DW, Li X, Aga M & Bradley JM. (2014). Intraocular pressure homeostasis: maintaining balance in a high-pressure environment. J Ocul Pharmacol Ther 30, 94–101. [PubMed: 24401029]

Adapala RK, Thoppil RJ, Luther DJ, Paruchuri S, Meszaros JG, Chilian WM & Thodeti CK. (2013). TRPV4 channels mediate cardiac fibroblast differentiation by integrating mechanical and soluble signals. J Mol Cell Cardiol 54, 45–52. [PubMed: 23142541]

Albarran-Juarez J, Iring A, Wang S, Joseph S, Grimm M, Strilic B, Wettschureck N, Althoff TF & Offermanns S. (2018). Piezo1 and Gq/G11 promote endothelial inflammation depending on flow pattern and integrin activation. J Exp Med 215, 2655–2672. [PubMed: 30194266]

Bae C, Sachs F & Gottlieb PA. (2011). The mechanosensitive ion channel Piezo1 is inhibited by the peptide GsMTx4. Biochemistry 50, 6295–6300. [PubMed: 21696149]

Beech DJ & Kalli AC. (2019). Force Sensing by Piezo Channels in Cardiovascular Health and Disease. Arterioscler Thromb Vasc Biol 39, 2228–2239. [PubMed: 31533470]

Besch SR, Suchyna T & Sachs F. (2002). High-speed pressure clamp. Pflugers Arch 445, 161–166. [PubMed: 12397401]

Boussommier-Calleja A, Bertrand J, Woodward DF, Ethier CR, Stamer WD & Overby DR. (2012). Pharmacologic manipulation of conventional outflow facility in ex vivo mouse eyes. Invest Ophthalmol Vis Sci 53, 5838–5845. [PubMed: 22807298]

Bradley JM, Kelley MJ, Zhu X, Anderssohn AM, Alexander JP & Acott TS. (2001). Effects of mechanical stretching on trabecular matrix metalloproteinases. Invest Ophthalmol Vis Sci 42, 1505–1513. [PubMed: 11381054]

Brohawn SG, Su Z & MacKinnon R. (2014). Mechanosensitivity is mediated directly by the lipid membrane in TRAAK and TREK1 K+ channels. Proc Natl Acad Sci U S A 111, 3614–3619. [PubMed: 24550493]

Carreon TA, Castellanos A, Gasull X & Bhattacharya SK. (2017). Interaction of cochlin and mechanosensitive channel TREK-1 in trabecular meshwork cells influences the regulation of intraocular pressure. Sci Rep 7, 452. [PubMed: 28352076]

Chen Y, Gao J, Li L, Sellitto C, Mathias RT, Donaldson PJ & White TW. (2019). The Ciliary Muscle and Zonules of Zinn Modulate Lens Intracellular Hydrostatic Pressure Through Transient Receptor Potential Vanilloid Channels. Invest Ophthalmol Vis Sci 60, 4416–4424. [PubMed: 31639828]

Lonsdale J, Thomas J, Salvatore M et al. (2013). The Genotype-Tissue Expression (GTEx) project. Nat Genet 45, 580–585. [PubMed: 23715323]

Corrigan MA, Johnson GP, Stavenschi E, Riffault M, Labour MN & Hoey DA. (2018). TRPV4-mediates oscillatory fluid shear mechanotransduction in mesenchymal stem cells in part via the primary cilium. Sci Rep 8, 3824. [PubMed: 29491434]

Coste B, Mathur J, Schmidt M, Earley TJ, Ranade S, Petrus MJ, Dubin AE & Patapoutian A. (2010). Piezo1 and Piezo2 are essential components of distinct mechanically activated cation channels. Science 330, 55–60. [PubMed: 20813920]

Cox CD, Bae C, Ziegler L, Hartley S, Nikolova-Krstevski V, Rohde PR, Ng CA, Sachs F, Gottlieb PA & Martinac B. (2016). Removal of the mechanoprotective influence of the cytoskeleton reveals PIEZO1 is gated by bilayer tension. Nat Commun 7, 10366. [PubMed: 26785635]

Cox CD & Gottlieb PA. (2019). Amphipathic molecules modulate PIEZO1 activity. Biochem Soc Trans 47, 1833–1842. [PubMed: 31754715]

Del Marmol JI, Touhara KK, Croft G & MacKinnon R. (2018). Piezo1 forms a slowly-inactivating mechanosensory channel in mouse embryonic stem cells. Elife 7.

Douguet D & Honore E. (2019). Mammalian Mechanoelectrical Transduction: Structure and Function of Force-Gated Ion Channels. Cell 179, 340–354. [PubMed: 31585078]

Faralli JA, Filla MS, McDowell CM & Peters DM. (2020). Disruption of fibronectin fibrillogenesis affects intraocular pressure (IOP) in BALB/cJ mice. PLoS One 15, e0237932. [PubMed: 32822410]

Faralli JA, Filla MS & Peters DM. (2019). Effect of alphavbeta3 Integrin Expression and Activity on Intraocular Pressure. Invest Ophthalmol Vis Sci 60, 1776–1788. [PubMed: 31022732]

Filla MS, Faralli JA, Peotter JL & Peters DM. (2017). The role of integrins in glaucoma. Exp Eye Res 158, 124–136. [PubMed: 27185161]

Filosa JA, Yao X & Rath G. (2013). TRPV4 and the regulation of vascular tone. J Cardiovasc Pharmacol 61, 113–119. [PubMed: 23107877]

Friedrich EE, Hong Z, Xiong S, Zhong M, Di A, Rehman J, Komarova YA & Malik AB. (2019). Endothelial cell Piezo1 mediates pressure-induced lung vascular hyperpermeability via disruption of adherens junctions. Proc Natl Acad Sci U S A 116, 12980–12985. [PubMed: 31186359]

Gasull X, Ferrer E, Llobet A, Castellano A, Nicolás JM, Palés J, Gual A. (2003). Cell membrane stretch modulates the high-conductance Ca2+-activated K+ channel in bovine trabecular meshwork cells. Invest Ophthalmol Vis Sci 44, 706–14. [PubMed: 12556402]

Gilchrist CL, Leddy HA, Kaye L, Case ND, Rothenberg KE, Little D, Liedtke W, Hoffman BD & Guilak F. (2019). TRPV4-mediated calcium signaling in mesenchymal stem cells regulates aligned collagen matrix formation and vinculin tension. Proc Natl Acad Sci U S A 116, 1992–1997. [PubMed: 30674675]

Gottlieb PA, Bae C & Sachs F. (2012). Gating the mechanical channel Piezo1: a comparison between whole-cell and patch recording. Channels (Austin) 6, 282–289. [PubMed: 22790451]

Gottlieb PA & Sachs F. (2012). Piezo1: properties of a cation selective mechanical channel. Channels (Austin) 6, 214–219. [PubMed: 22790400]

Iring A, Jin YJ, Albarran-Juarez J, Siragusa M, Wang S, Dancs PT, Nakayama A, Tonack S, Chen M, Kunne C, Sokol AM, Gunther S, Martinez A, Fleming I, Wettschureck N, Graumann J, Weinstein LS & Offermanns S. (2019). Shear stress-induced endothelial adrenomedullin signaling regulates vascular tone and blood pressure. J Clin Invest 129, 2775–2791. [PubMed: 31205027]

Johnstone M, Martin E & Jamil A. (2011). Pulsatile flow into the aqueous veins: manifestations in normal and glaucomatous eyes. Exp Eye Res 92, 318–327. [PubMed: 21440541]

Johnstone MA. (2004). The aqueous outflow system as a mechanical pump: evidence from examination of tissue and aqueous movement in human and non-human primates. J Glaucoma 13, 421–438. [PubMed: 15354083]

Jonas JB, Weber P, Nagaoka N & Ohno-Matsui K. (2017). Glaucoma in high myopia and parapapillary delta zone. PLoS One 12, e0175120. [PubMed: 28380081]

Keller KE, Bhattacharya SK, Borras T, Brunner TM, Chansangpetch S, Clark AF, Dismuke WM, Du Y, Elliott MH, Ethier CR, Faralli JA, Freddo TF, Fuchshofer R, Giovingo M, Gong H, Gonzalez P, Huang A, Johnstone MA, Kaufman PL, Kelley MJ, Knepper PA, Kopczynski CC, Kuchtey JG, Kuchtey RW, Kuehn MH, Lieberman RL, Lin SC, Liton P, Liu Y, Lutjen-Drecoll E, Mao W, Masis-Solano M, McDonnell F, McDowell CM, Overby DR, Pattabiraman PP, Raghunathan VK, Rao PV, Rhee DJ, Chowdhury UR, Russell P, Samples JR, Schwartz D, Stubbs EB, Tamm ER, Tan JC, Toris CB, Torrejon KY, Vranka JA, Wirtz MK, Yorio T, Zhang J, Zode GS, Fautsch MP, Peters DM, Acott TS & Stamer WD. (2018). Consensus recommendations for trabecular meshwork cell isolation, characterization and culture. Exp Eye Res 171, 164–173. [PubMed: 29526795]

Kim JG, Park SW, Byun D, Choi WS, Sung DJ, Shin KC, Kim HJ, Leem YE, Kang JS, Cho H, Kim B, Cho SI & Bae YM. (2016). Fluid flow facilitates inward rectifier K(+) current by convectively restoring [K(+)] at the cell membrane surface. Sci Rep 6, 39585. [PubMed: 28004830]

Kim SE, Coste B, Chadha A, Cook B & Patapoutian A. (2012). The role of Drosophila Piezo in mechanical nociception. Nature 483, 209–212. [PubMed: 22343891]

Kohler R & Hoyer J. (2007). Role of TRPV4 in the Mechanotransduction of Shear Stress in Endothelial Cells In TRP Ion Channel Function in Sensory Transduction and Cellular Signaling Cascades, ed. Liedtke WB & Heller S. Boca Raton (FL).

Krizaj D (2019). No cell is an island: trabecular meshwork ion channels as sensors of the ambient milieu, vol. 3 Kugler Publications Amsterdam.

Kumar S, Shah S, Deutsch ER, Tang HM & Danias J. (2013). Triamcinolone acetonide decreases outflow facility in C57BL/6 mouse eyes. Investigative ophthalmology & visual science 54, 1280–1287. [PubMed: 23322580]

Lacroix JJ, Botello-Smith WM & Luo Y. (2018). Probing the gating mechanism of the mechanosensitive channel Piezo1 with the small molecule Yoda1. Nat Commun 9, 2029. [PubMed: 29795280]

Last JA, Pan T, Ding Y, Reilly CM, Keller K, Acott TS, Fautsch MP, Murphy CJ & Russell P. (2011). Elastic modulus determination of normal and glaucomatous human trabecular meshwork. Invest Ophthalmol Vis Sci 52, 2147–2152. [PubMed: 21220561]

Lewis AH, Cui AF, McDonald MF & Grandl J. (2017). Transduction of Repetitive Mechanical Stimuli by Piezo1 and Piezo2 Ion Channels. Cell Rep 19, 2572–2585. [PubMed: 28636944]

Lewis AH & Grandl J. (2015). Mechanical sensitivity of Piezo1 ion channels can be tuned by cellular membrane tension. Elife 4.

Lakk M & Krizaj D. (2020). Mechanoreciprocity requires interactions between TRPV4 channels, the Rho pathway and actin cytoskeleton. BioRxiv.2020.08.11.247171

Li C, Rezania S, Kammerer S, Sokolowski A, Devaney T, Gorischek A, Jahn S, Hackl H, Groschner K, Windpassinger C, Malle E, Bauernhofer T & Schreibmayer W. (2015). Piezo1 forms mechanosensitive ion channels in the human MCF-7 breast cancer cell line. Sci Rep 5, 8364. [PubMed: 25666479]

Li G, Lee C, Agrahari V, Wang K, Navarro I, Sherwood JM, Crews K, Farsiu S, Gonzalez P & Lin C-W. (2019). In vivo measurement of trabecular meshwork stiffness in a corticosteroid-induced ocular hypertensive mouse model. Proceedings of the National Academy of Sciences 116, 1714–1722.

Li J, Hou B, Tumova S, Muraki K, Bruns A, Ludlow MJ, Sedo A, Hyman AJ, McKeown L, Young RS, Yuldasheva NY, Majeed Y, Wilson LA, Rode B, Bailey MA, Kim HR, Fu Z, Carter DA, Bilton J, Imrie H, Ajuh P, Dear TN, Cubbon RM, Kearney MT, Prasad RK, Evans PC, Ainscough JF & Beech DJ. (2014). Piezo1 integration of vascular architecture with physiological force. Nature 515, 279–282. [PubMed: 25119035]

Lu H, Dong J, Zhang Y, Li C, Yu Q & Tang W. (2014). Pathological changes in primary cilia: A novel mechanism of graft cholangiopathy caused by prolonged cold preservation in a rat model of orthotopic liver transplantation. Biosci Trends 8, 206–211. [PubMed: 25224626]

Luo N, Conwell MD, Chen X, Kettenhofen CI, Westlake CJ, Cantor LB, Wells CD, Weinreb RN, Corson TW, Spandau DF, Joos KM, Iomini C, Obukhov AG & Sun Y. (2014). Primary cilia signaling mediates intraocular pressure sensation. Proc Natl Acad Sci U S A 111, 12871–12876. [PubMed: 25143588]

Luo N, West CC, Murga-Zamalloa CA, Sun L, Anderson RM, Wells CD, Weinreb RN, Travers JB, Khanna H & Sun Y. (2012). OCRL localizes to the primary cilium: a new role for cilia in Lowe syndrome. Hum Mol Genet 21, 3333–3344. [PubMed: 22543976]

McDonnell F, Perkumas KM, Ashpole NE, Kalnitsky J, Sherwood JM, Overby DR & Stamer WD. (2020). Shear Stress in Schlemm's Canal as a Sensor of Intraocular Pressure. Sci Rep 10, 5804. [PubMed: 32242066]

Molnar T, Yarishkin O, Iuso A, Barabas P, Jones B, Marc RE, Phuong TT & Krizaj D. (2016). Store-Operated Calcium Entry in Muller Glia Is Controlled by Synergistic Activation of TRPC and Orai Channels. J Neurosci 36, 3184–3198. [PubMed: 26985029]

Moroni M, Servin-Vences MR, Fleischer R, Sanchez-Carranza O & Lewin GR. (2018). Voltage gating of mechanosensitive PIEZO channels. Nat Commun 9, 1096. [PubMed: 29545531]

Murthy SE, Dubin AE & Patapoutian A. (2017). Piezos thrive under pressure: mechanically activated ion channels in health and disease. Nat Rev Mol Cell Biol 18, 771–783. [PubMed: 28974772]

Overby DR, Stamer WD & Johnson M. (2009). The changing paradigm of outflow resistance generation: towards synergistic models of the JCT and inner wall endothelium. Exp Eye Res 88, 656–670. [PubMed: 19103197]

Patel GC, Phan TN, Maddineni P, Kasetti RB, Millar JC, Clark AF & Zode GS. (2017). Dexamethasone-induced ocular hypertension in mice: Effects of myocilin and route of administration. The American journal of pathology 187, 713–723. [PubMed: 28167045]

Peterson JA, Tian B, Bershadsky AD, Volberg T, Gangnon RE, Spector I, Geiger B & Kaufman PL. (1999). Latrunculin-A increases outflow facility in the monkey. Invest Ophthalmol Vis Sci 40, 931–941. [PubMed: 10102290]

Phuong TTT, Redmon SN, Yarishkin O, Winter JM, Li DY & Krizaj D. (2017). Calcium influx through TRPV4 channels modulates the adherens contacts between retinal microvascular endothelial cells. J Physiol 595, 6869–6885. [PubMed: 28949006]

Qiu Z, Guo J, Kala S, Zhu J, Xian Q, Qiu W, Li G, Zhu T, Meng L, Zhang R, Chan HC, Zheng H, Sun L. (2019). The Mechanosensitive Ion Channel Piezo1 Significantly Mediates In Vitro Ultrasonic Stimulation of Neurons. iScience 21, 448–457. [PubMed: 31707258]

Ranade SS, Qiu Z, Woo SH, Hur SS, Murthy SE, Cahalan SM, Xu J, Mathur J, Bandell M, Coste B, Li YS, Chien S & Patapoutian A. (2014). Piezo1, a mechanically activated ion channel, is required for vascular development in mice. Proc Natl Acad Sci U S A 111, 10347–10352. [PubMed: 24958852]

Ranade SS, Syeda R & Patapoutian A. (2015). Mechanically Activated Ion Channels. Neuron 87, 1162–1179. [PubMed: 26402601]

Rao PV, Pattabiraman PP & Kopczynski C. (2017). Role of the Rho GTPase/Rho kinase signaling pathway in pathogenesis and treatment of glaucoma: Bench to bedside research. Exp Eye Res 158, 23–32. [PubMed: 27593914]

Retailleau K, Duprat F, Arhatte M, Ranade SS, Peyronnet R, Martins JR, Jodar M, Moro C, Offermanns S, Feng Y, Demolombe S, Patel A & Honore E. (2015). Piezo1 in Smooth Muscle Cells Is Involved in Hypertension-Dependent Arterial Remodeling. Cell Rep 13, 1161–1171. [PubMed: 26526998]

Rode B, Shi J, Endesh N, Drinkhill MJ, Webster PJ, Lotteau SJ, Bailey MA, Yuldasheva NY, Ludlow MJ, Cubbon RM, Li J, Futers TS, Morley L, Gaunt HJ, Marszalek K, Viswambharan H, Cuthbertson K, Baxter PD, Foster R, Sukumar P, Weightman A, Calaghan SC, Wheatcroft SB, Kearney MT & Beech DJ. (2017). Piezo1 channels sense whole body physical activity to reset cardiovascular homeostasis and enhance performance. Nat Commun 8, 350. [PubMed: 28839146]

Ryskamp DA, Frye AM, Phuong TT, Yarishkin O, Jo AO, Xu Y, Lakk M, Iuso A, Redmon SN, Ambati B, Hageman G, Prestwich GD, Torrejon KY & Krizaj D. (2016). TRPV4 regulates calcium homeostasis, cytoskeletal remodeling, conventional outflow and intraocular pressure in the mammalian eye. Sci Rep 6, 30583. [PubMed: 27510430]

Ryskamp DA, Jo AO, Frye AM, Vazquez-Chona F, MacAulay N, Thoreson WB & Krizaj D. (2014). Swelling and eicosanoid metabolites differentially gate TRPV4 channels in retinal neurons and glia. J Neurosci 34, 15689–15700. [PubMed: 25411497]

Sakamoto E, Ishida W, Sumi T, Kishimoto T, Tada K, Fukuda K, Yoneda T, Kuroiwa H, Terao E, Fujisawa Y, Nakakura S, Jian K, Okumichi H, Kiuchi Y & Fukushima A. (2019). Evaluation of offset of conjunctival hyperemia induced by a Rho-kinase inhibitor; 0.4% Ripasudil ophthalmic solution clinical trial. Sci Rep 9, 3755. [PubMed: 30842572]

Servin-Vences MR, Moroni M, Lewin GR & Poole K. (2017). Direct measurement of TRPV4 and PIEZO1 activity reveals multiple mechanotransduction pathways in chondrocytes. Elife 6.

Sharma S, Goswami R, Zhang DX & Rahaman SO. (2019). TRPV4 regulates matrix stiffness and TGFbeta1-induced epithelial-mesenchymal transition. J Cell Mol Med 23, 761–774. [PubMed: 30450767]

Shepard AR, Millar JC, Pang I-H, Jacobson N, Wang W-H & Clark AF. (2010). Adenoviral gene transfer of active human transforming growth factor-β2 elevates intraocular pressure and reduces outflow facility in rodent eyes. Investigative ophthalmology & visual science 51, 2067–2076. [PubMed: 19959644]

Sherwood JM, Reina-Torres E, Bertrand JA, Rowe B & Overby DR. (2016). Measurement of Outflow Facility Using iPerfusion. PLoS One 11, e0150694. [PubMed: 26949939]

Sherwood JM, Stamer WD & Overby DR. (2019). A model of the oscillatory mechanical forces in the conventional outflow pathway. J R Soc Interface 16, 20180652. [PubMed: 30958169]

Solis AG, Bielecki P, Steach HR, Sharma L, Harman CCD, Yun S, de Zoete MR, Warnock JN, To SDF, York AG, Mack M, Schwartz MA, Dela Cruz CS, Palm NW, Jackson R & Flavell RA. (2019). Mechanosensation of cyclical force by PIEZO1 is essential for innate immunity. Nature 573, 69–74. [PubMed: 31435009]

Soni H, Peixoto-Neves D, Matthews AT & Adebiyi A. (2017). TRPV4 channels contribute to renal myogenic autoregulation in neonatal pigs. Am J Physiol Renal Physiol 313, F1136–F1148. [PubMed: 28768667]

Suchyna TM, Tape SE, Koeppe RE 2nd, Andersen OS, Sachs F & Gottlieb PA. (2004). Bilayer-dependent inhibition of mechanosensitive channels by neuroactive peptide enantiomers. Nature 430, 235–240. [PubMed: 15241420]

Swain SM, Romac JM, Shahid RA, Pandol SJ, Liedtke W, Vigna SR & Liddle RA. (2020). TRPV4 channel opening mediates pressure-induced pancreatitis initiated by Piezo1 activation. J Clin Invest 130, 2527–2541. [PubMed: 31999644]

Syeda R, Florendo MN, Cox CD, Kefauver JM, Santos JS, Martinac B & Patapoutian A. (2016). Piezo1 Channels Are Inherently Mechanosensitive. Cell Rep 17, 1739–1746. [PubMed: 27829145]

Syeda R, Xu J, Dubin AE, Coste B, Mathur J, Huynh T, Matzen J, Lao J, Tully DC, Engels IH, Petrassi HM, Schumacher AM, Montal M, Bandell M & Patapoutian A. (2015). Chemical activation of the mechanotransduction channel Piezo1. Elife 4.

Thodeti CK, Matthews B, Ravi A, Mammoto A, Ghosh K, Bracha AL & Ingber DE. (2009). TRPV4 channels mediate cyclic strain-induced endothelial cell reorientation through integrin-to-integrin signaling. Circ Res 104, 1123–1130. [PubMed: 19359599]

Toft-Bertelsen TL, Yarishkin O, Redmon S, Phuong TTT, Krizaj D & MacAulay N. (2019). Volume sensing in the transient receptor potential vanilloid 4 ion channel is cell type-specific and mediated by an N-terminal volume-sensing domain. J Biol Chem 294, 18421–18434. [PubMed: 31619514]

Tran VT, Ho PT, Cabrera L, Torres JE & Bhattacharya SK. (2014). Mechanotransduction channels of the trabecular meshwork. Curr Eye Res 39, 291–303. [PubMed: 24215462]

Turner DC, Edmiston AM, Zohner YE, Byrne KJ, Seigfreid WP, Girkin CA, Morris JS & Downs JC. (2019). Transient Intraocular Pressure Fluctuations: Source, Magnitude, Frequency, and Associated Mechanical Energy. Invest Ophthalmol Vis Sci 60, 2572–2582. [PubMed: 31212310]

Vahabikashi A, Park CY, Perkumas K, Zhang Z, Deurloo EK, Wu H, Weitz DA, Stamer WD, Goldman RD, Fredberg JJ & Johnson M. (2019). Probe Sensitivity to Cortical versus Intracellular Cytoskeletal Network Stiffness. Biophys J 116, 518–529. [PubMed: 30685055]

Watanabe H, Vriens J, Prenen J, Droogmans G, Voets T & Nilius B. (2003). Anandamide and arachidonic acid use epoxyeicosatrienoic acids to activate TRPV4 channels. Nature 424, 434–438. [PubMed: 12879072]

Wu J, Young M, Lewis AH, Martfeld AN, Kalmeta B & Grandl J. (2017). Inactivation of Mechanically Activated Piezo1 Ion Channels Is Determined by the C-Terminal Extracellular Domain and the Inner Pore Helix. Cell Rep 21, 2357–2366. [PubMed: 29186675]

WuDunn D (2009). Mechanobiology of trabecular meshwork cells. Exp Eye Res 88, 718–723. [PubMed: 19071113]

Xia Y, Fu Z, Hu J, Huang C, Paudel O, Cai S, Liedtke W & Sham JS. (2013). TRPV4 channel contributes to serotonin-induced pulmonary vasoconstriction and the enhanced vascular reactivity in chronic hypoxic pulmonary hypertension. Am J Physiol Cell Physiol 305, C704–715. [PubMed: 23739180]

Yarishkin O, Phuong TTT, Bretz CA, Olsen KW, Baumann JM, Lakk M, Crandall A, Heurteaux C, Hartnett ME & Krizaj D. (2018). TREK-1 channels regulate pressure sensitivity and calcium signaling in trabecular meshwork cells. J Gen Physiol 150, 1660–1675. [PubMed: 30446509]

Yarishkin O, Phuong TTT & Krizaj D. (2019). Trabecular Meshwork TREK-1 Channels Function as Polymodal Integrators of Pressure and pH. Invest Ophthalmol Vis Sci 60, 2294–2303. [PubMed: 31117121]

Zeng WZ, Marshall KL, Min S, Daou I, Chapleau MW, Abboud FM, Liberles SD & Patapoutian A. (2018). PIEZOs mediate neuronal sensing of blood pressure and the baroreceptor reflex. Science 362, 464–467. [PubMed: 30361375]

**Key points**

- Trabecular meshwork (TM) is a highly mechanosensitive tissue in the eye that regulates intraocular pressure through the control of aqueous humor drainage.
- Its dysfunction underlies the progression of glaucoma but neither the mechanisms through which TM cells sense pressure nor their role in aqueous humor outflow are understood at the molecular level.
- We identified the Piezo1 channel as a key TM transducer of tensile stretch, shear flow and pressure.
- Its activation resulted in intracellular signals that altered organization of the cytoskeleton and cell-extracellular matrix contacts and modulated the trabecular component of aqueous outflow whereas another channel, TRPV4, mediated a delayed mechanoresponse.
- This study helps elucidate basic mechanotransduction properties that may contribute to intraocular pressure regulation in the vertebrate eye.

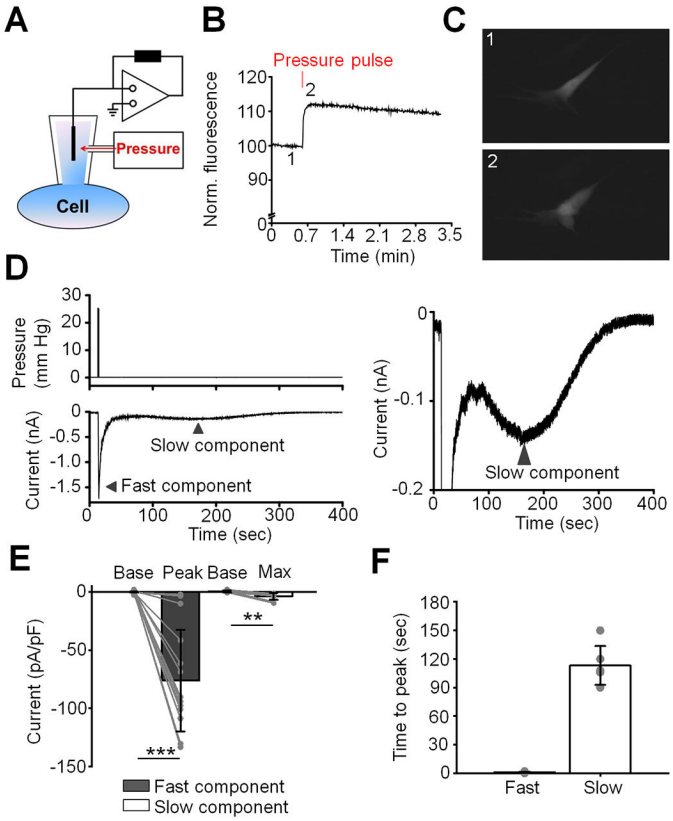


**Figure 1. Two kinetically distinct components of pressure-induced current.**

**(A)** Schematic diagram of the setup. **(B)** A representative trace of calcein fluorescence illustrating effect of pressure pulse. Positive changes in fluorescence indicate at an increase in cell volume. **(C)** A representative fluorescent image demonstrating change in cell volume after application of a pressure pulse. Images were taken at the corresponding time points shown in (B)**. (D)** A representative trace illustrating the fast and the slow components *(lower trace)* of the response to pressure *(upper trace)*. The right panel is the Y-axis expansion of the trace shown in the left panel. The holding potential was −40 mV. **(E)** Quantification of the magnitude of the fast and the slow responses. Shown are the means ± SD of baseline current (base) measured before application of the pressure pulse and the current measured at the peak and the maximum of the fast and the slow components, respectively. The gray symbols indicate individual values. $^{**}p = 0.0033$, $^{***}p < 0.00001$, paired-sample *t*-test; N = 2 different donors' eyes, $n = 15$ and n = 9 cells for the fast and the slow components, respectively. **(F)** Bar graphs summarizing kinetics of fast and slow components. Results obtained from cells isolated from two different donors' eyes were pooled. Shown is the mean ± SD of time measured between application of the pressure pulse and when current reaches the maximum value. Grey symbols represent individual values. n = 17 cells and n = 6 cells for fast and slow response, respectively.

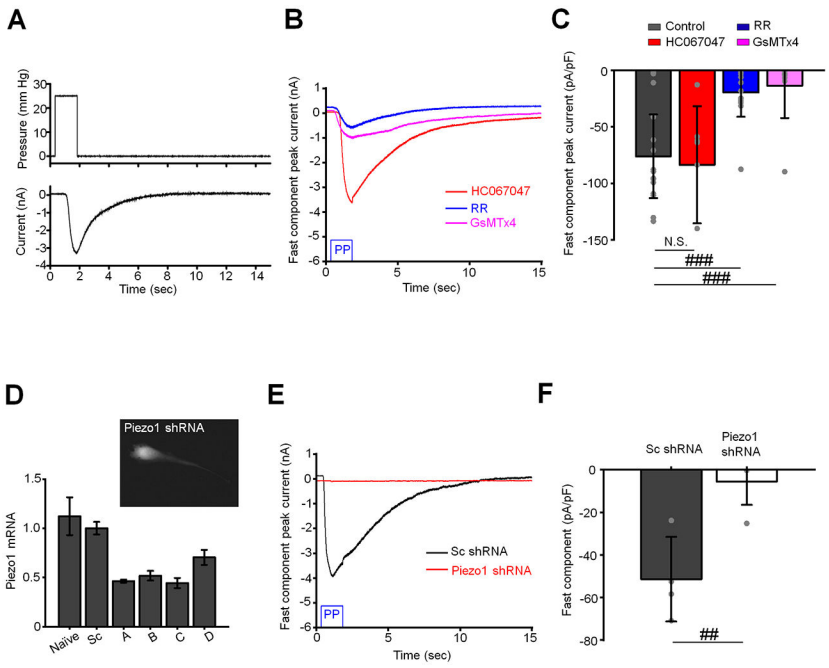


**Figure 2. Piezo1 mediates the fast component of pressure-induced current.**

**(A)** A representative trace of the fast component. The waveform of the pressure pulse is shown above the trace. **(B)** The fast component is attenuated by non-selective Piezo1 antagonists ruthenium red (RR, 10 μM) and GsMTx4 (5 μM), but not a TRPV4 antagonist HC06047 (5 μM). Shown are representative traces. **(C)** Quantification of results illustrated in B. Shown is the mean ± SD values of the fast response. The response was calculated by subtracting the baseline current from the peak current. $^{N.S.}p = 0.7252$; $^{###}p = 0.00012$ and p = 0.0010 for control *vs.* HC067047, contro *vs.* RR, and control *vs.* GsMTx4, respectively. Two-sample *t*-test. N = 2 eyes, n = 15, n = 7, n = 15, and n = 9 cells for untreated (control) cells and cells treated with HC067047, RR and GsMTx4, respectively. **(D)** Validation of Piezo1 shRNA constructs by Q-PCR analysis. Shown are the mean ± SD. N = 3 independent experiments. The insert is a representative fluorescent image of a TM cell overexpressing Piezo1 shRNA-mCherry construct. **(E)** The fast component is attenuated by in cells overexpressing Piezo1 shRNA but not sc shRNA. Shown are representative traces. **(F)** Bar graphs summarizing effects of Piezo1 knockdown on the fast component of pressure response. The response was calculated by subtracting the baseline current from the peak current. Shown are the means ± SD. $^{##}p = 0.0031$, two-sample *t*-test. n = 4 cells and n = 4 cells for scrambled control (Sc-shRNA) and Piezo1-shRNA overexpressing cells, respectively. The holding potential in A-C and E and F was −40 mV.

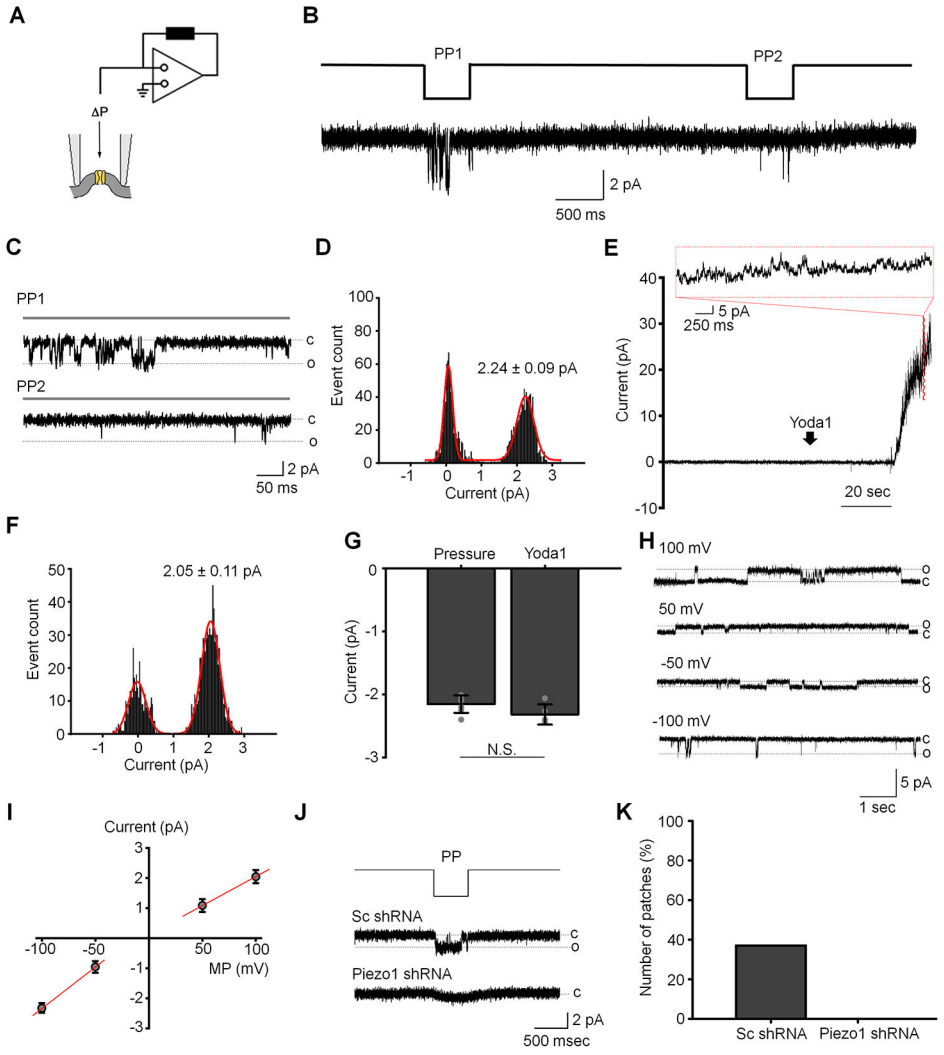


**Figure 3. Activity of Piezo1-like channel in TM cells.**

**(A)** A schematic of the inside-out patch clamp configuration. Negative pressure (ΔP) was delivered through the patch pipette. **(B)** A duplet pressure pulse (−80 mm Hg, 500 ms) triggered the activity of a rapid activating and inactivating channel in excised inside-out plasma membrane patches. **(C)** Expanded traces of single channel activity recorded during the first (PP1) and the second (PP2) pressure pulse application. The trace is an extract of the trace shown in B. Dashed lines indicate closed (c) and open (o) states of the channel. **(D)** A representative histogram of unitary current amplitude of the pressure-activated channel. The solid red line is a fitting of the Gaussian equation through the experimental data ($\chi^2$ 18.24, degrees of freedom = 121, R-Square (COD) = 93%). The current amplitude of the closed levels is 0.063 ± 0.055 pA. The bin-width is 0.03 pA and sampling time 8 sec. The membrane potential was −100 mV. **(E)** A representative recording illustrating induction of multiple channel activity by Yoda1 (10 μM). The insert shown above the trace is an expansion of the outlined extract. The membrane potential was 100 mV. **(F)** A representative histogram of unitary current amplitude of the channel activated by Yoda1. The solid line is a fitting of the Gaussian equation through the experimental data ($\chi^2$ = 8.19, degrees of

freedom = 115, R-Square (COD) = 93%). The bin-width is 0.03 pA. The current amplitude of the closed levels is −0.023 ± 0.18 pA. The membrane potential was −100 mV. **(G)** The comparative analysis of the amplitude of pressure- and Yoda1-induced current recorded at the membrane potential −100 mV. Shown are the mean ± SD. $^{N.S.}p = 0.08$. Two-sample *t*-test; n = 7 and 5 patches, respectively. **(H)** Original registrations of Yoda1-induced single channel activity at different membrane potentials. **(I)** The I-V relations for the Yoda1-induced single channel current. Shown are the mean ± SD *(symbols)* and linear regression through the data *(solid red lines)*. **(J)** Occurrence of the Piezo1-like channel reduced in cells overexpressing Piezo1 shRNA compared to control cells overexpressing scramble shRNA. Shown are representative current traces. **(K)** Quantification of the effect of Piezo1 knockdown on the occurrence of Piezo1-like channel. The membrane potential was −100 mV.

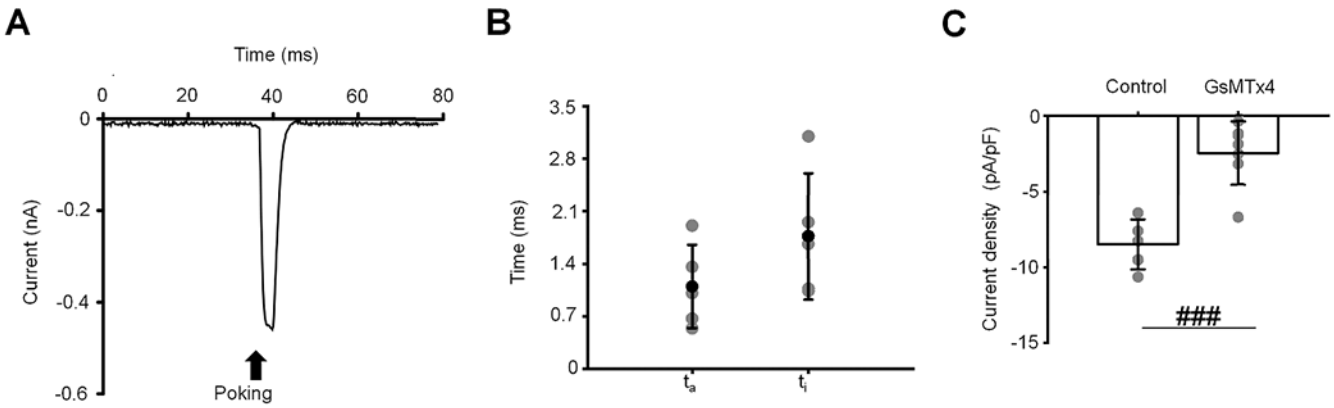


**Figure 4. Piezo1 mediates the indentation-evoked current with msec kinetics.**

**(A)** A representative trace of the whole-cell current induced by cell poking in TM cells. Poking is indicated by an arrow. The holding potential was −40 mV **(B)** The activation ($\tau_a$) and inactivation ($\tau_i$) time constants of poking-induced current. Time constants are represented as the mean ± SD. **(C)** Current density. Shown are the mean ± SD. $^{###}p$ = 0.0003; two-samples *t*-test; n = 4 cells and n = 7 cells for control and GsMTx4 (5 μM), respectively. Gray symbols in the middle and the right plots represent individual values.

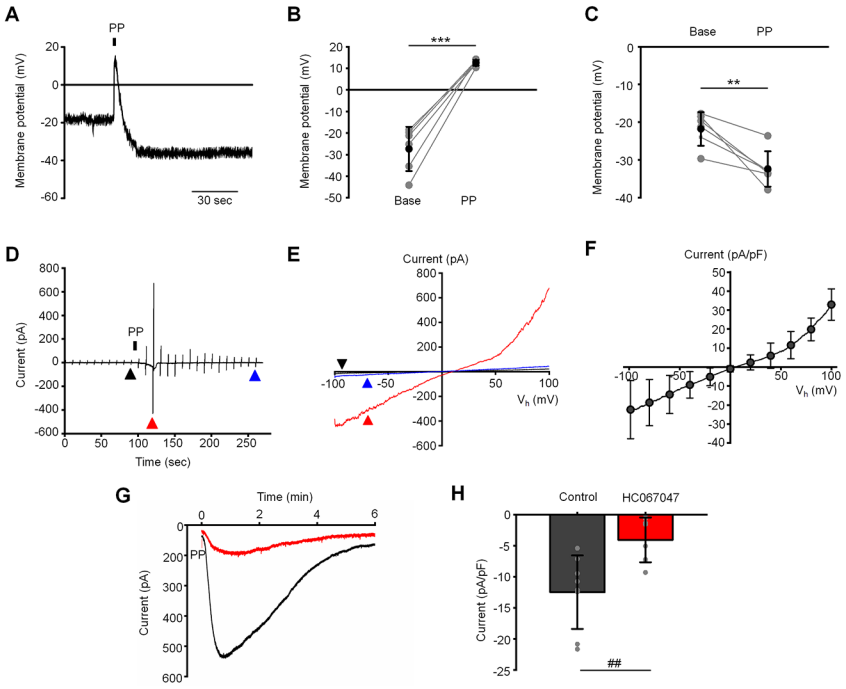


**Figure 5. Cation selectivity of the fast and the slow component.**

**(A)** Representative recording illustrating effects of the pressure pulse (PP) on the membrane potential. **(B)** Summary for depolarizing effect of the fast component and **(C)** following hyperpolarizing shift of the membrane potential. $^{***}p = 0.00006$ and $^{**}p = 0.0058$ for B and C, respectively. Paired-sample *t*-test. n = 6 cells and n = 6 cells for B and C, respectively. Base: baseline levels recording before application of pressure. **(D)** Original registration of the slow component current under $K^+$-free conditions. The current was elicited by voltage RAMPs ascending from −100 mV to 100 mV applied at 0.1 Hz. The holding potential was 0 mV. **(E)** The I-V curves of current recorded at the indicated *(triangles)* time points in the trace shown in D. **(F)** Averaged I-C curve of the pressure-induced current recorded under $K^+$-free conditions. Shown are the mean ± SD (symbols) and the averaged I-V curve. N = 6 cells. **(G)** Original registrations of the slow component illustrating the inhibitory effect of HC06047 (5 μM). Both cells did not exhibit the fast response to the pressure pulse. The holding potential was −100 mV. A single pressure pulse (PP) was applied at the indicated time. **(H)** Summary for results illustrated in D. Shown is the mean ± SD of the slow component. The response was calculated by subtracting the baseline current from the peak current. $^{\#\#}p = 0.0040$, two-sample *t*-test. n = 8 cells and n = 8 cells for untreated (control) and HC067047-treated cells, respectively.

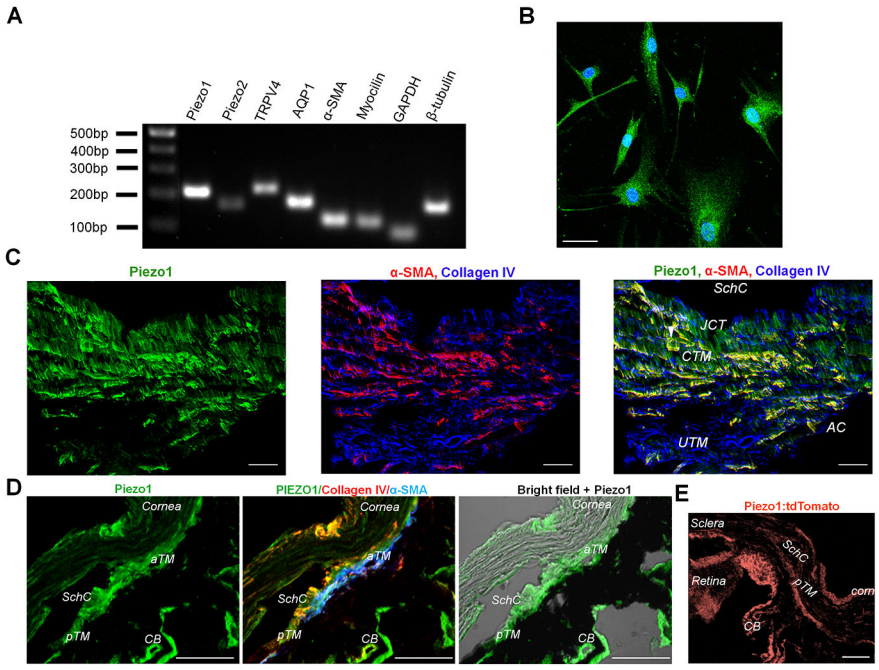


**Figure 6. Molecular expression of Piezo1 channel in human TM.**

**(A)** Representative Q-PCR results demonstrating expression of mRNA encoding *PIEZO1, PIEZO2, TRPV4* and TM markers aquaporin 1 (AQP1), α smooth muscle actin (α-SMA) and Myocilin. **(B)** ICC results confirm the expression of Piezo1 protein in primary cultures of human TM cells. Scale bar is 50 μm. **(C)** Representative fluorescent IHC images illustrating the expression of Piezo1 (Green) in the anterior segment of the human eye. The tissue was co-stained for TM markers α-SMA (*red*) and Collagen IV (*blue*). *SchC*: the canal of Schlemm; *TM*: the trabecular meshwork. *AC*: Anterior chamber; *JCT*: Juxtacanalicular tissue; *CTM*: Corneoscleral trabecular meshwork; *UTM*: Uveal trabecular meshwork. Magnification bars: 20 μm. **(D)** Expression of Piezo1 in the anterior segment of the mouse eye. Shown are representative IHC results of co-staining of the anterior segment with anti-Piezo1, anti-collagen IV and anti-α-SMA antibody. *aTM:* anterior TM, *pTM:* posterior TM, *SchC:* the Schlemm's canal, *CB:* ciliary body. Scale bar is 50 μm. **(E)** The Piezo1$^{P1\text{-}tdTomato}$ mouse confirmed Piezo1 promoter activity in the trabecular meshwork and ciliary body. *aTM:* anterior TM, *pTM:* posterior TM, *SchC:* the Schlemm's canal, *CB:* ciliary body. Scale bar in D and E is 50 μm.

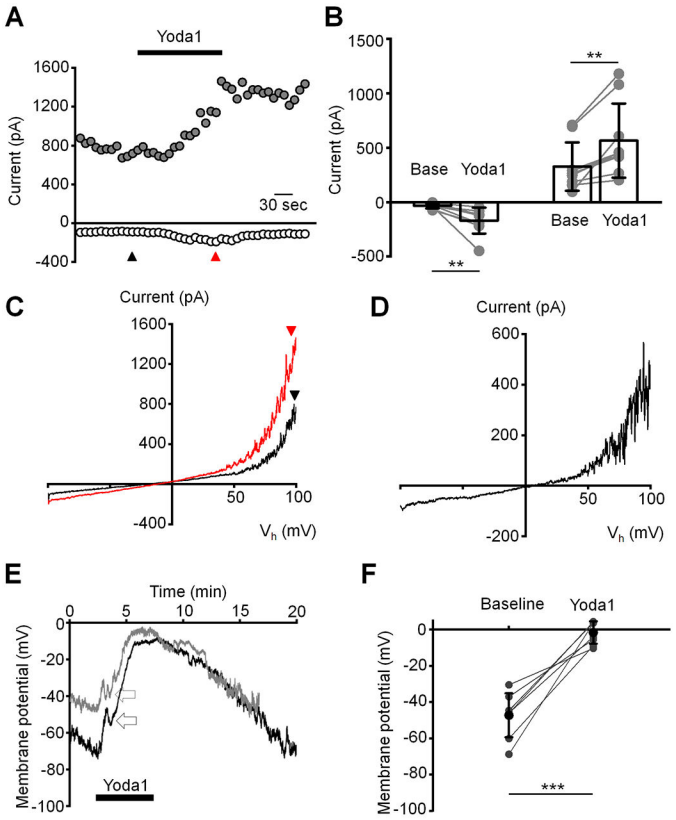


**Figure 7. Agonist-induced activation of Piezo1 in TM cells.**

**(A)** Representative time course of the whole-cell current illustrating effect of Yoda1 (5 μM). Shown are the amplitude of current recorded at the holding potentials −100 mV *(open symbols)* and 100 mV *(filled symbols)*. **(B)** Bar graphs summarizing effect of Yoda1 on the whole-cell current recorded at the holding potential −100 mV *(left)* and 100 mV *(right)*. Shown are the mean ± SD . $^{**}p = 0.0064$ and $p = 0.0032$ for base *vs.* Yoda1 (negative current) and base *vs.* Yoda1 (positive current), respectively. Paired-sample *t*-test; N = 2 different donors eyes, n = 9 cells. Base: baseline current recorded before application of Yoda1. **(C)** I-V curves of baseline (*black*; taken at the indicated time point in A) and Yoda1-evoked (*red*; taken at the indicated time point in A). **(D)** The current-voltage relationship of Yoda1-induced current reconstructed from I-V curves shown in C by subtracting the baseline I-V curve from the I-V curve of current recorded in the presence of Yoda1. **(E)** Effects of Yoda1 on the plasma membrane potential of TM cells. The left panel: representative traces. Time of Yoda1 (10 μM) application is indicated by the bar. Arrowheads point at transient repolarizing component of the response to Yoda1. **(F)** The quantification of Yoda1-induced depolarization of the plasma membrane potential. Shown are the mean ± SD. $^{***}p = 0.00006$; paired-sample *t*-test; n = 8 cells. Gray symbols represent individual values.

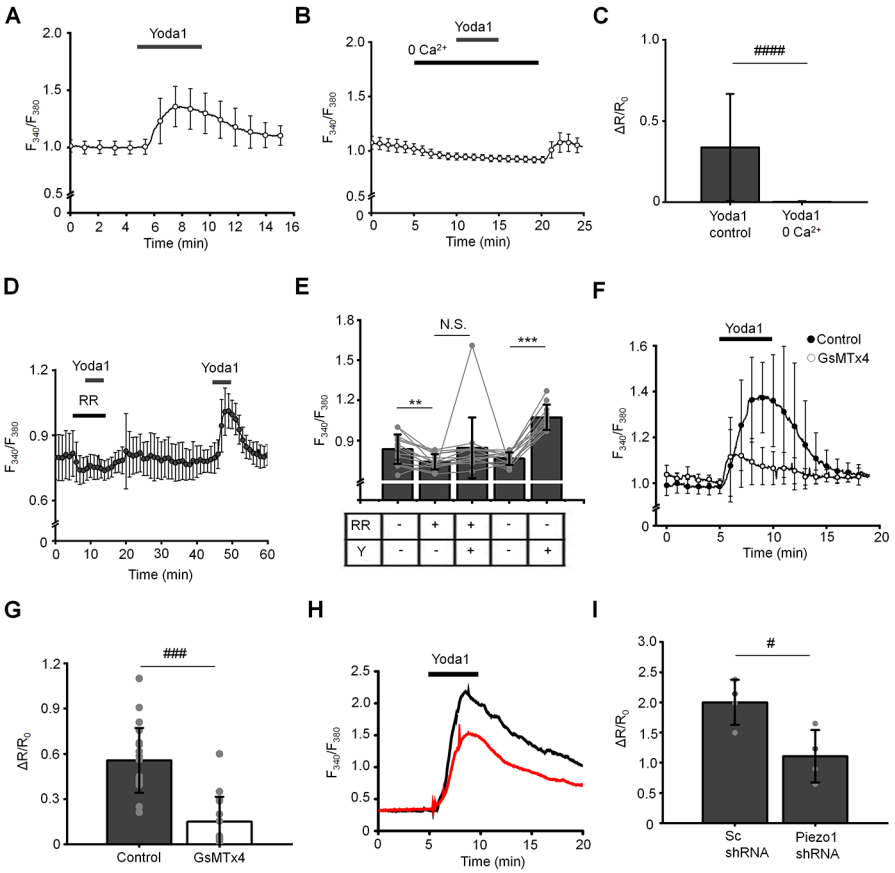


**Figure 8. Activity of Piezo1 is functionally coupled to elevation of intracellular calcium ions in TM cells.**

**(A and B)** Yoda1 triggers a robust increase in $[Ca^{2+}]_i$ that was abolished in $Ca^{2+}$-free extracellular solution. N = 2 eyes, n = 39 cells for control and N = 2, n = 61 cells for "0 $Ca^{2+}$" conditions, respectively. **(C)** Bar graphs summarizing results illustrating in A and B. Shown the mean ± SD. $^{\#\#\#\#}$, $p < 0.00001$; n > 50 cells, paired-sample *t*-test. **(D)** Ruthenium red (RR; 10 μM) abolished effect of Yoda1 (10 μM) on $[Ca^{2+}]_i$. **(E)** Bar graphs summarizing results shown in D. Shown the mean ± SD. $^{N.S.}p = 0.1378$; $^{**}p = 0.0018$; $^{***}p < 0.00001$. n = 14 cells, paired-sample *t*-test. RR: ruthenium red, Y: Yoda1. **(F)** Elevation of $[Ca^{2+}]_i$ by Yoda1 (10 μM) is attenuated in the presence of GsMTx4 (5 μM). Shown are averaged traces (the mean ± SEM) for untreated control cells (n = 17 cells; filled symbols) and GsMTx4-treated cells (n = 15 cells). **(G)** Bar graphs summarizing inhibitory effect of GsMTx4 on Yoda1-induced elevation of $[Ca^{2+}]_i$. $^{\#\#\#}p < 0.00001$, two-sample *t*-test. **(H)** Representative $F_{340}/F_{380}$ nm traces illustrating effects of Piezo1 shRNA on Yoda1-mediated elevation of $[Ca^{2+}]_i$. The black trace represents control (Sc) and the red trace represents Piezo1 shRNA. **(I)** Bar graphs summarizing results shown in H. Shown the mean ± SD. $^{\#}p = 0.0204$; N = 4 coverslips per each condition (Sc shRNA: 24 - 45 cells per coverslip; Piezo1 shRNA: 7 – 17 cells per coverslip), two-sample *t*-test.

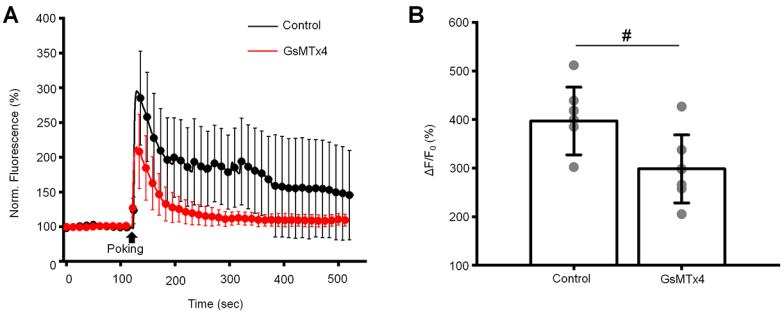


**Figure 9. The indentation-induced calcium response is mediated by Piezo1**

**(A)** Cell poking induces elevation of $[Ca^{2+}]_i$ in TM cells. The left panel: averaged traces of Fluo-4 obtained from untreated (control) and cells treated with GsMTx4 (5 μM). Shown are the mean ± SD. **(B)** Quantification of inhibitory effect GsMTx4 on poking-induced elevation of $[Ca^{2+}]_i$. Shown are the mean ± SD. $^{\#}p$ =0.0173; two-samples *t*-test; n = 8 cells and n = 7 cells for control and Yoda1 plots, respectively. Gray symbols represent individual values.

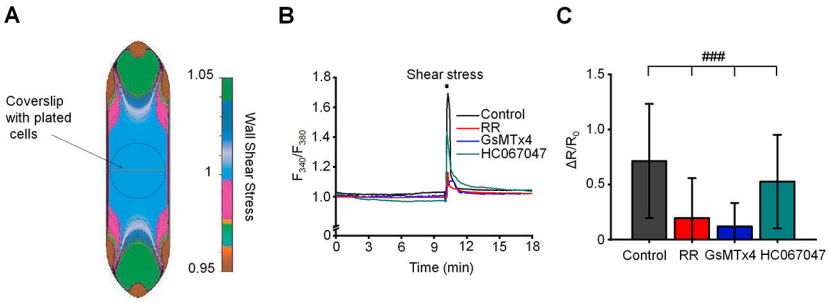


**Figure 10. Piezo1 couples fluid shear stress to elevation of $[Ca^{2+}]_i$ in TM cells.**

**(A)** Distribution of wall shear stress in the flow chamber. The image was adapted from Warner Instruments. **(B)** Representative traces of normalized $F_{340/380}$ ratio illustrating effect of laminar flow stress on $[Ca^{2+}]_i$. 0.5 dyn/cm$^2$ shear stress was applied for 10 sec. **(C)** Bar graphs summarizing results shown in B. $^{###}p < 0.00001$, n = 77 cells, n = 62 cells, n = 39 cells, and n = 69 cells for untreated (control), ruthenium red treated, GsMTx4 treated and HC067047-treated cells, respectively. ANOVA multiple comparisons test, Tukey's test was applied for means comparison, R-Square = 76 %. Shown are the mean ± SD. RR, GsMTx4, and HC067047 were applied at concentrations 30 μM, 5 μM, and 5 μM respectively.

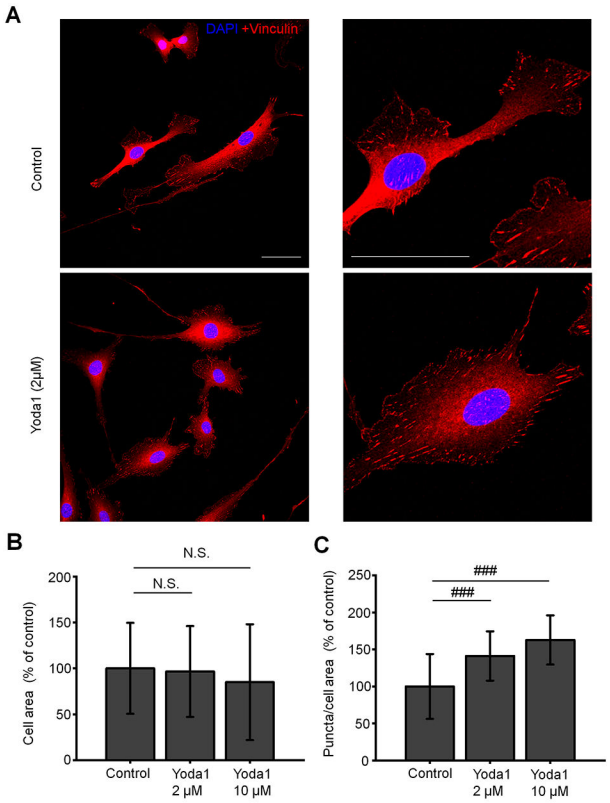


**Figure 11. Piezo1 mediates reorganization of focal adhesions.**

**(A)** Representative examples of untreated (control) and Yoda1-treated TM cells immunolabeled for vinculin. Yoda1 was applied at a concentration of 2 μM for 1h. Scale bar is 50 μm. **(B)** Magnified images of cells shown in A. Scale bar is 50 μm. **(C – D)** Bar graphs summarizing effects of Yoda1 on the cells area and the number of vocal adhesions. $^{N.S.}p$ = 0.7170 and p = 0.1564 for control *vs.* Yoda1 2 μM and control *vs.* Yoda1 10 μM, respectively; $^{###}p$ = 0.00002 (control vs. Yoda1 2 μM) and p = 0.00002 (control vs. Yoda1 10μM); n = 41 cells, n = 65 cells, n = 59 cells, cells for control, 2 μM Yoda1 and 10 μM Yoda1-treated cells, respectively. Two-sample *t*-test. Shown are the mean ± SD.

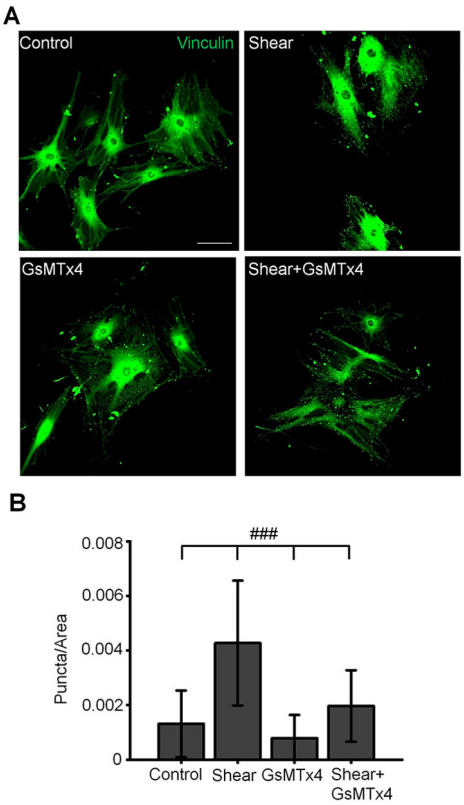


**Figure 12. Shear stress-induced reorganization of focal adhesions require the activity of Piezo1.**

**(A)** Representative examples of TM cells immunolabeled for vinculin. Scale bar is 50 μm. **(B)** Bar graphs summarizing effects of shear stress and GsMTx4 on a number of vocal adhesions. $^{###}p < 0.00001$; n = 112, 120, 120 and 108 cells for control, shear, GsMTx4, and shear+GsMTx4 groups, respectively. ANOVA multiple comparisons test, Tukey's test was applied for means comparison, R-Square = 45 %. Shown are the mean ± SD. GsMTx4 (5 μM) was added to the perfusing solution 5 min prior to shear stress.

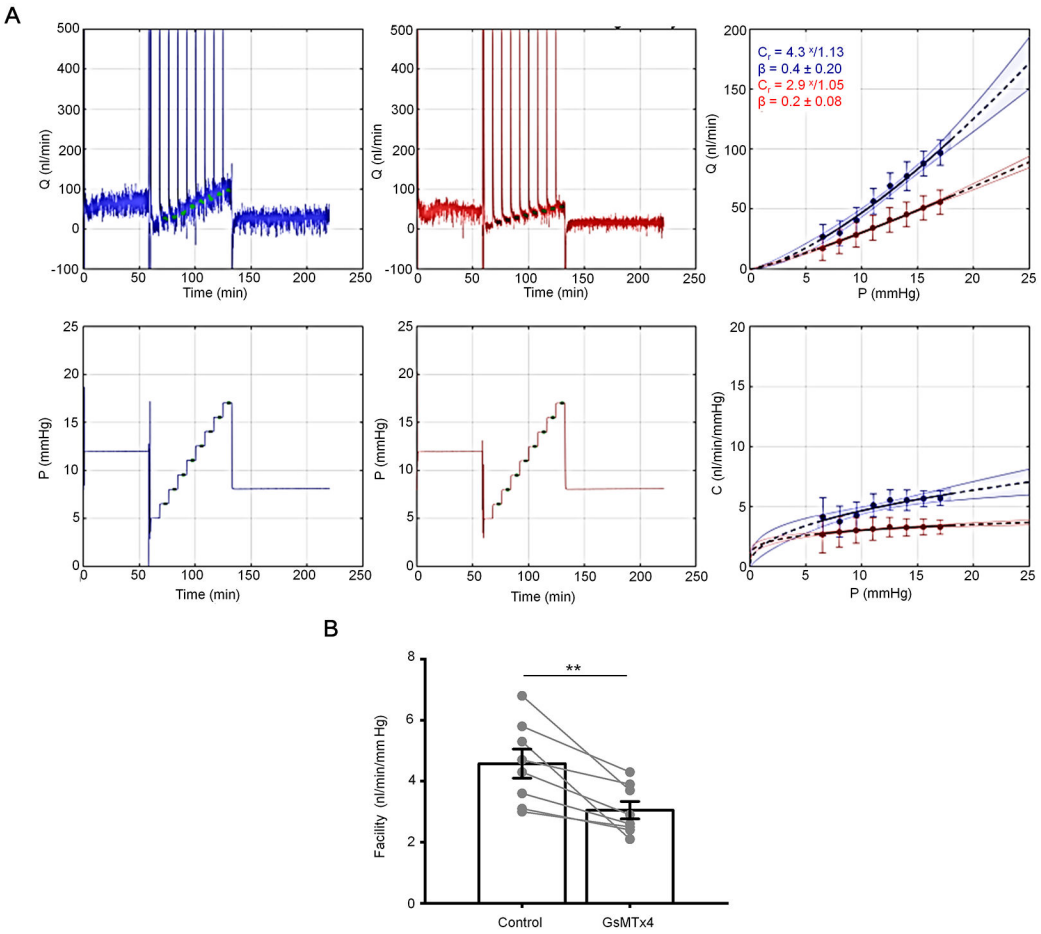


**Figure 13. The activity of Piezo1 regulates outflow facility of trabecular outflow pathway.**

**(A)** Shown are representative traces that depict flow (Q) and pressure (P) measured in perfused, enucleated and paired mouse eyes. Upper panels show flow rate as a function of time, and lower panels show corresponding pressure steps as a function of time. Traces show GsMTx4-treated *(red)* and untreated *(blue)* eyes. **(B)** Overlaid traces from both GsMTx4-treated and control treatments. Upper panel depicts flow as a function of pressure steps, and lower panel depicts outflow facility (C) as a function of pressure steps, where C is Q/P. The exponent β characterizes the nonlinearity of the flow-pressure relationship. $C_r$ is the outflow facility calculated at the reference pressure of 8 mmHg. **(C)** GsMTx4 treatment reduced conventional, pressure-dependent outflow compared with no drug treatment ($^{**}p = 0.0047$, n = 8 eyes, paired t-test). Mean ± SD. GsMTx4 was applied at a concentration 6 μM.